Functional redundancy between flavodiiron proteins and NDH-1 in Synechocystis sp. PCC 6803

Lauri Nikkanen, Anita Santana Sánchez, Maria Ermakova, Matthias Rögner, Laurent Cournac, Yagut Allahverdiyeva

the plant journal

SEB SOCIETY FOR EXPERIMENTAL BIOLOGY

The Plant Journal (2020) doi: 10.1111/tpj.14812

Functional redundancy between flavodiiron proteins and NDH-1 in *Synechocystis* sp. PCC 6803

Lauri Nikkanen[1], Anita Santana Sánchez[1], Maria Ermakova[1,†], Matthias Rögner[2], Laurent Cournac[3] and Yagut Allahverdiyeva[1]*

[1]*Molecular Plant Biology, Department of Biochemistry, University of Turku, Turku, Finland,*
[2]*Plant Biochemistry, Faculty of Biology & Biotechnology, Ruhr-University Bochum, Bochum, Germany, and*
[3]*Eco&Sols, University of Montpellier, IRD, CIRAD, INRAE, Institut Agro, Montpellier, France*

Received 15 January 2020; revised 30 April 2020; accepted 5 May 2020.
*For correspondence (e-mail allahve@utu.fi).
†Present address: Australian Research Council Centre of Excellence for Translational Photosynthesis, Division of Plant Science, Research School of Biology, The Australian National University, Acton, Australia

SUMMARY

In oxygenic photosynthetic organisms, excluding angiosperms, flavodiiron proteins (FDPs) catalyze light-dependent reduction of O_2 to H_2O. This alleviates electron pressure on the photosynthetic apparatus and protects it from photodamage. In *Synechocystis* sp. PCC 6803, four FDP isoforms function as hetero-oligomers of Flv1 and Flv3 and/or Flv2 and Flv4. An alternative electron transport pathway mediated by the NAD(P)H dehydrogenase-like complex (NDH-1) also contributes to redox hemostasis and the photoprotection of photosynthesis. Four NDH-1 types have been characterized in cyanobacteria: NDH-1_1 and NDH-1_2, which function in respiration; and NDH-1_3 and NDH-1_4, which function in CO_2 uptake. All four types are involved in cyclic electron transport. Along with single FDP mutants (Δ*flv1* and Δ*flv3*) and the double NDH-1 mutants (Δ*d1d2*, which is deficient in NDH-$1_{1,2}$ and Δ*d3d4*, which is deficient in NDH-$1_{3,4}$), we studied triple mutants lacking one of Flv1 or Flv3, and NDH-$1_{1,2}$ or NDH-$1_{3,4}$. We show that the presence of either Flv1/3 or NDH-$1_{1,2}$, but not NDH-$1_{3,4}$, is indispensable for survival during changes in growth conditions from high CO_2/moderate light to low CO_2/high light. Our results show functional redundancy between FDPs and NDH-$1_{1,2}$ under the studied conditions. We suggest that ferredoxin probably functions as a primary electron donor to both Flv1/3 and NDH-$1_{1,2}$, allowing their functions to be dynamically coordinated for efficient oxidation of photosystem I and for photoprotection under variable CO_2 and light availability.

Keywords: Flavodiiron proteins, Flv, NDH-1, photosynthesis, *Synechocystis* sp. PCC 6803, cyanobacteria, Mehler-like reaction, alternative electron transfer, photoprotection.

INTRODUCTION

Photosynthetic organisms have evolved a variety of different regulatory mechanisms, which are important for the protection of the photosynthetic machinery during rapid changes in environmental conditions. Fluctuating light intensities present particular risk to the photosystems due to over-reduction of the photosynthetic electron transport chain (PETC), particularly photosystem (PS) I (Allahverdiyeva *et al.*, 2015; Tiwari *et al.*, 2016; Shimakawa *et al.*, 2016). To counter this, cyanobacteria, algae and plants (excluding angiosperms) employ C-type flavodiiron proteins (FDPs) as a strong photoprotective electron sink, directing excess photosynthetic electrons from downstream of PSI to O_2 (Helman *et al.*, 2003; Allahverdiyeva *et al.*, 2013; Gerotto *et al.*, 2016; Ilik *et al.*, 2017; Chaux *et al.*, 2017; Jokel *et al.*, 2018; Alboresi *et al.*, 2019). This process is referred to as the Mehler-like reaction and, in contrast to the Mehler reaction (Mehler, 1957), does not produce harmful reactive oxygen species (Vicente *et al.*, 2002; Brown *et al.*, 2019).

The genome of the β-cyanobacterium *Synechocystis* sp. PCC 6803 (hereafter *Synechocystis*) encodes four isoforms of FDPs, namely Flv1–4, which function in O_2 photoreduction mainly as hetero-oligomers consisting of either Flv1 and Flv3 or Flv2 and Flv4 (Zhang *et al.*, 2004; Mustila *et al.*, 2016; Santana-Sanchez *et al.*, 2019). Recently, we showed that under air level [CO_2], Flv1/3 and Flv2/4 hetero-oligomers function in a coordinated and interdependent manner: Flv1/3 stimulates strong but transient O_2 photoreduction upon the onset of illumination or during increases in light intensity, while Flv2/4 hetero-oligomers catalyze a slower and

limited steady-state reduction of O_2, also using electrons downstream of PSI (Santana-Sanchez *et al.*, 2019). In elevated [CO_2] and in air [CO_2] at alkaline pH 9, the *flv4-flv2* operon encoding Flv2, Flv4 and the Sll0218 protein is down-regulated (Zhang *et al.*, 2009; Santana-Sanchez *et al.*, 2019). Nevertheless, a low level of Flv1/3 in elevated [CO_2] stimulates strong steady-state O_2 photoreduction, whereas in air [CO_2] at pH 9, Flv1/3 is solely responsible for strong but transient O_2 photoreduction (Santana-Sanchez *et al.*, 2019). Whilst *in vitro* assays showed that homo-oligomers of recombinant Flv1, Flv3 and Flv4 can reduce O_2 with NADH and/or NADPH (Vicente *et al.*, 2002; Shimakawa *et al.*, 2015; Brown *et al.*, 2019), ferredoxin-$NADP^+$-reductase (FNR) and reduced ferredoxin (Fd) are yet to be considered as possible donors to FDPs. Moreover, the use of *Synechocystis* mutants solely overexpressing Flv1 or Flv3 clearly demonstrated that, in contrast to *in vitro* experiments, homo-oligomers of Flv3 or Flv1 are not involved in O_2 photoreduction *in vivo* (Mustila *et al.*, 2016). Thus, the electron donor to FDPs remains to be elucidated *in vivo*.

In cyanobacteria, photosynthetic and respiratory electron transfer reactions coexist on thylakoid membranes and are intricately linked, necessitating strict regulation (Mullineaux, 2014). The NAD(P)H dehydrogenase-like complex 1 (NDH-1, photosynthetic complex I) is mainly localized in thylakoid membranes and involved in several bioenergetic reactions, including cyclic electron transfer (CET) around PSI, respiration and CO_2 acquisition via the carbon concentrating mechanism (CCM) (for reviews see Battchikova *et al.*, 2011; Ma and Ogawa, 2015; Burnap *et al.*, 2015; Peltier *et al.*, 2016). The NDH-1 complex is present as several forms with distinct physiological roles: the NDH-1_1 type features the subunits NdhD1 and NdhF1 and functions as complex I of the respiratory electron transfer chain (Zhang *et al.*, 2004; He *et al.*, 2015; Saura and Kaila, 2019); the NDH-1_2 form features the NdhD2 subunit instead of NdhD1, but it remains unclear whether NDH-1_1 and NDH-1_2 serve different physiological functions (Peltier *et al.*, 2016). The NDH-1_3 and NDH-1_4 forms that comprise low-C_i-inducible, high-affinity CO_2 acquisition subunits NdhD3, NdhF3, CupA and CupS, or constitutive, low-affinity CO_2 acquisition subunits NdhD4, NdhF4 and CupB, respectively, function in conversion of CO_2 to HCO_3^- (Ohkawa *et al.*, 2000a,b; Shibata *et al.*, 2001; Zhang *et al.*, 2004; Burnap *et al.*, 2013; Han *et al.*, 2017; Schuller *et al.*, 2019). This process is possibly enabled by alkaline pockets at the thylakoid membrane created by NDH-1 proton pumping (Kaplan and Reinhold, 1999). All four NDH-1 types catalyze CET from Fd to plastoquinone (PQ), which is coupled to the pumping of $4H^+/2e^-$ into the thylakoid lumen (He *et al.*, 2015; Laughlin *et al.*, 2019; Schuller *et al.*, 2019; Saura and Kaila, 2019). However, CET mediated by NDH-$1_{3,4}$ is minor in comparison to CET mediated by NDH-$1_{1,2}$ (Bernat *et al.*, 2011).

In the current study, we aim to elucidate how the electron transport pathways mediated by FDPs and NDH-1 cooperate to allow the maintenance of redox poise between the PETC, respiration, CCM and CO_2 fixation in the Calvin–Benson–Bassham cycle (CBB) under variable light and C_i availability. To this end, we employed both biophysical and biochemical methods to characterize various *Synechocystis* mutant strains with combined deficiencies of both FDP and NDH-1 pathways. Our results provide convincing evidence for the presence of either Flv1/3 or NDH-$1_{1,2}$, but not NDH-$1_{3,4}$, being indispensable for the survival of *Synechocystis* cells under transitions from high [CO_2] conditions to the combined stress conditions of air [CO_2] and high light. We show that the dynamically coordinated and cooperative function of Flv1/3 and NDH-$1_{1,2}$ is required for the photoprotection of the photosynthetic apparatus of *Synechocystis* cells and discuss the molecular mechanisms involved. We suggest that this coordination is enabled by a shared electron donor, as Fd probably functions as the main reductant of both Flv1/3 and NDH-$1_{1,2}$, although the possible contribution of NADPH as a donor cannot be fully excluded.

RESULTS

Simultaneous inactivation of Flv1/3 and NDH-$1_{1,2}$ is lethal upon shift from high to air [CO_2] and high light

To examine whether the simultaneous inactivation of NDH-1 and FDPs has an adverse effect on cell survival, we monitored the growth of *Synechocystis* wild-type (WT) and various mutant strains lacking (i) either Flv1 or Flv3 (Δ*flv1* and Δ*flv3*, respectively; Helman *et al.*, 2003), (ii) both NdhD1 and NdhD2 (Δ*d1d2*, deficient in NDH-1_1 and NDH-1_2; Ohkawa *et al.*, 2000b), (iii) both NdhD3 and NdhD4 (Δ*d3d4*, deficient in NDH-1_3 and NDH-1_4; Ohkawa *et al.*, 2000b), as well as triple mutants with combined deficiencies of both pathways (Δ*flv1 d1d2*, Δ*flv3 d1d2*, Δ*flv1 d3d4*, Δ*flv3 d3d4*) in conditions of differing CO_2 availability and light intensity. The triple mutants exhibited similar or slightly slower growth compared with the WT and other mutant strains under high [CO_2] (3% CO_2) and moderate light (ML, intensity of 50 μmol photons m^{-2} sec^{-1} of photosynthetically active radiance) (Figure 1a). We also detected no substantial difference in growth when the 3% CO_2/ML pre-grown cells were diluted [optical density $(OD)_{750}$ = 0.1] and shifted to air [CO_2] conditions under constant light intensity (Figure 1b; Figure S1a,c). In contrast, when cultures pre-grown in 3% [CO_2]/ML were diluted (OD_{750} = 0.1) and subjected simultaneously to air [CO_2] and high light stress conditions (HL, intensity of 220 μmol photons m^{-2} sec^{-1}), the growth of both Δ*flv3 d1d2* and Δ*flv1 d1d2* strains was completely inhibited (Figure 1d). Importantly, Δ*flv1*, Δ*flv3* and Δ*d1d2* strains demonstrated growth similar to WT cells under air [CO_2]/HL conditions.

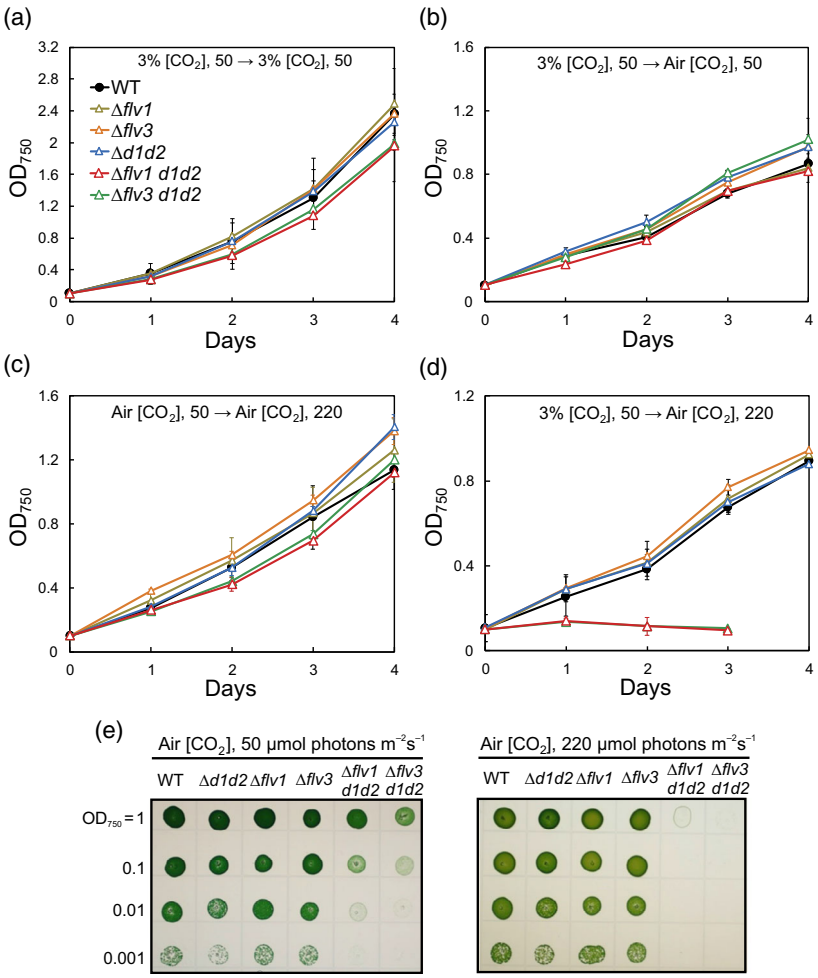

Figure 1. Growth of wild-type (WT) and mutant strains under different experimental conditions. All experimental cultures were started from pre-cultures adjusted to OD_{750} = 0.1.
(a) Cells were pre-cultivated under 3% $[CO_2]$/moderate light (ML) (50 μmol photons m^{-2} sec^{-1}), adjusted to OD_{750} = 0.1 and grown in the same conditions.
(b) Cells were pre-cultivated under 3% $[CO_2]$/ML and shifted to air $[CO_2]$/ML.
(c) Cells were pre-cultivated under air $[CO_2]$/ML and shifted to air $[CO_2]$/high light (HL) 220 μmol photons m^{-2} sec^{-1}).
(d) Cells were pre-cultivated under 3% $[CO_2]$/ML and shifted to air $[CO_2]$/HL. Values presented in a–d are means of three independent biological replicates ± SE.
(e) Growth of WT and mutant cells on agar plates containing BG-11. Cells grown under 3% $[CO_2]$/ML were harvested and spotted on BG-11 agar plates in 10-fold dilution series starting at OD_{750} = 1, incubation was under air $[CO_2]$/ML and air $[CO_2]$/HL for 7 days. See also Figure S1.

We next examined whether pre-adaptation to air $[CO_2]$ would rescue the growth arrest. When cells previously adapted to air $[CO_2]$/ML were diluted (OD_{750} = 0.1) and shifted to air $[CO_2]$/HL, no differences in growth patterns between the strains were detected (Figure 1c). Importantly, the triple mutants lacking either Flv1 or Flv3 and NDH-$1_{3,4}$ (Δ*flv1 d3d4* and Δ*flv3 d3d4* strains) did not show a lethal phenotype after a shift from 3% $[CO_2]$/ML to air $[CO_2]$/HL, although somewhat reduced growth was observed compared with the control strains (Figure S1b,d). This suggests that, under the studied conditions, cooperation of Flv1/3 with NDH-$1_{3,4}$ complexes is not as crucial as with NDH-$1_{1,2}$. Our attempts to create M55/Δ*flv1* and M55/Δ*flv3* double mutants lacking either Flv1 or Flv3 and the central membrane component of the NDH-1 complex, NdhB, were both unsuccessful. We were unable to obtain any M55/Δ*flv1* colonies and the M55/Δ*flv3* mutant strain could not be segregated (Figure S1e), suggesting that the absence of both Flv1/3 and NDH-1 disrupts essential cell metabolism.

We also studied the growth of the mutant strains on agar plates containing BG-11 (Figure 1e). For these experiments, 3% CO_2/ML-grown cells were diluted and grown on plates under either air $[CO_2]$/ML or air $[CO_2]$/HL conditions for 7 days. The Δ*flv1* and Δ*flv3* and Δ*d1d2* mutants did not exhibit any visible differences in growth capacity under these conditions in comparison with the WT. In contrast, the growth of the Δ*flv1 d1d2* and Δ*flv3 d1d2* triple mutants was strongly reduced under air $[CO_2]$/ML, while no growth was detected under air $[CO_2]$/HL (Figure 1e). The Δ*flv1 d3d4* and Δ*flv3 d3d4* triple mutants demonstrated a slow growth phenotype, similarly to that previously reported for Δ*d3d4* on agar plates (Ohkawa *et al.*, 2000b).

As the growth phenotypes of Δ*flv1* and Δ*flv3*, Δ*flv1 d1d2* and Δ*flv3 d1d2* were similar under all conditions, we only included Δ*flv3* and Δ*flv3 d1d2* in the majority of subsequent experiments.

Either Flv1/3 or NDH-$1_{1,2}$ is required for the oxidation of PSI during sudden increases in light intensity

The lethal phenotype observed upon the shift to air $[CO_2]$/HL, which was caused by the simultaneous impairment of

the Mehler-like reaction catalyzed by Flv1/3 (Helman *et al.*, 2003; Allahverdiyeva *et al.*, 2011, 2013) and by NDH-$1_{1,2}$ complex-mediated respiration and CET (Ohkawa *et al.*, 2000b; Bernat *et al.*, 2011) suggests a functional redundancy between these electron transport pathways. To investigate this possibility further, we used membrane inlet mass spectrometry (MIMS) to examine the kinetics of O_2 and CO_2 exchange upon HL illumination of dark-adapted WT and mutant cells grown for 4 days in air [CO_2]/ML. To distinguish O_2 uptake from photosynthetic gross O_2 evolution under illumination, we enriched cell suspensions with $^{18}O_2$ before the measurements. In dark-adapted WT cells, a transient peak in O_2 uptake occurs during the first minute of illumination (Figure 2a). We showed recently that this transient peak is attributed to the Mehler-like reaction catalyzed predominantly by Flv1/3 hetero-oligomers, while Flv2/4 hetero-oligomers mainly contribute to steady-state light-induced O_2 reduction in an interdependent manner (Santana-Sanchez *et al.*, 2019). In Δ*flv3* cells, light-induced O_2 reduction was almost abolished and only a slight impairment of the rate of photosynthetic gross O_2 evolution was observed in comparison with WT cells (Figure 2b). This result is in agreement with previous studies (Helman *et al.*, 2003; Allahverdiyeva *et al.*, 2013; Santana-Sanchez *et al.*, 2019).

In contrast to the WT, Δ*d1d2* cells lacked a fast decay phase of light-induced O_2 uptake during the first minute of illumination, demonstrating sustained O_2 photoreduction at high levels [approximately 75–100 μmol O_2 mg chlorophyll (Chl)$^{-1}$ h^{-1}] throughout the illumination period. Meanwhile, gross O_2 evolution was diminished nearly two-fold compared with the WT (Figure 2c). Thus, sustained O_2 photoreduction in Δ*d1d2* is not due to increased electron flow from PSII, but most probably due to increased activity of FDPs. Indeed, Δ*flv3 d1d2* mutant cells showed only minor light-induced O_2 uptake transiently during the first minute of illumination (Figure 2d). The Δ*flv3 d1d2* cells demonstrated slower induction of photosynthetic O_2 evolution following two-component kinetics, and slightly impaired steady-state gross O_2 evolution compared with WT (Figure 2d).

The initial peak in CO_2 uptake rate at the onset of illumination probably reflects activation of the CCM (Liran *et al.*, 2018). Accordingly, this initial peak is absent in the M55 mutant deficient in NDH-$1_{3,4}$ in addition to NDH-$1_{1,2}$, as well as in WT cells grown at pH 6 (Figure S2). No salient impairment of CCM was observed in any of the studied strains under air [CO_2]/ML, with CO_2 uptake rates peaking at approximately 1.5 mM CO_2 mg Chl^{-1} h^{-1}. In WT as well as in Δ*flv3*, CO_2 fixation is then induced and the respiratory compensation point surpassed after approximately 1 min of illumination (Figure 2a,b). However, in Δ*d1d2*, induction of CO_2 fixation is severely delayed and the cells only reached the compensation point at the end of the 5-min illumination period (Figure 2c). Intriguingly, although a slight delay was observed also in Δ*flv3 d1d2,* induction of CO_2 fixation was largely recovered in the triple mutant (Figure 2d).

These MIMS results indicated that combined deficiency of Flv1/3 and NDH-$1_{1,2}$ under standard growth conditions, air [CO_2]/ML, slightly perturbs photosynthetic electron transfer and the redox poise between the PETC and cytosolic sink reactions. Next, we examined the ability of the mutant strains to adjust their photosynthetic activity to variable light conditions by measuring Chl *a* fluorescence simultaneously with P700 redox changes in conditions where light intensity periodically fluctuated between low (25 μmol photons m^{-2} sec^{-1}, LL) and high irradiance (530 μmol photons m^{-2} sec^{-1}, HL). Cells lacking Flv3 suffered from transient PSI acceptor side limitation Y(NA) upon sudden increases in light intensity, resulting in delayed oxidation of PSI (Figure 3a), which is in line with

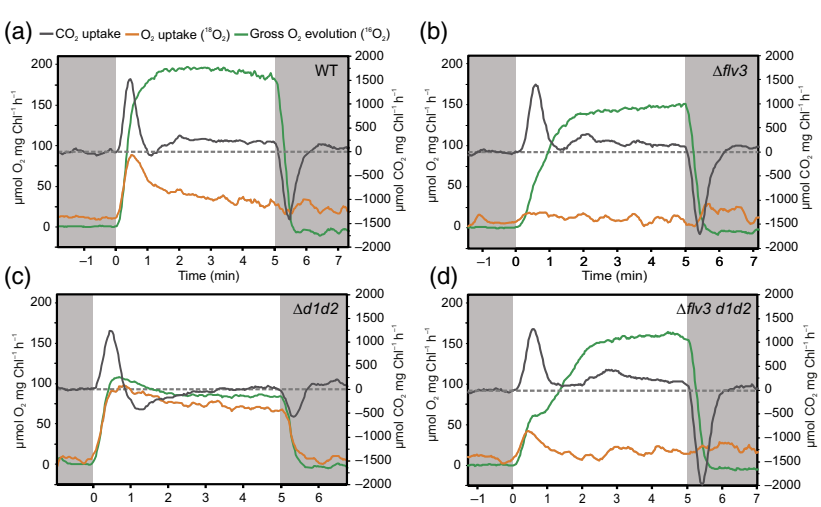

Figure 2. O_2 and CO_2 exchange rates in wild-type and mutant strains. Cells were grown in air [CO_2]/moderate light for 4 days, after which the cells were harvested and chlorophyll (Chl) *a* concentration adjusted to 10 μg ml^{-1} with fresh BG-11. Cells were dark-adapted for 15 min, and gas exchange was monitored by membrane inlet mass spectrometry over a 5-min illumination period with 500 μmol photons m^{-2} sec^{-1} of white actinic light. Before the measurements, samples were supplemented with $^{18}O_2$ at an equivalent concentration to $^{16}O_2$ to distinguish O_2 uptake from O_2 evolution, and with 1.5 mM $NaHCO_3$. Dashed line in each panel indicates the compensation point of CO_2 fixation (uptake rate equals respiratory rate). The experiment was repeated with three independent biological replicates, of which representative measurements are shown.

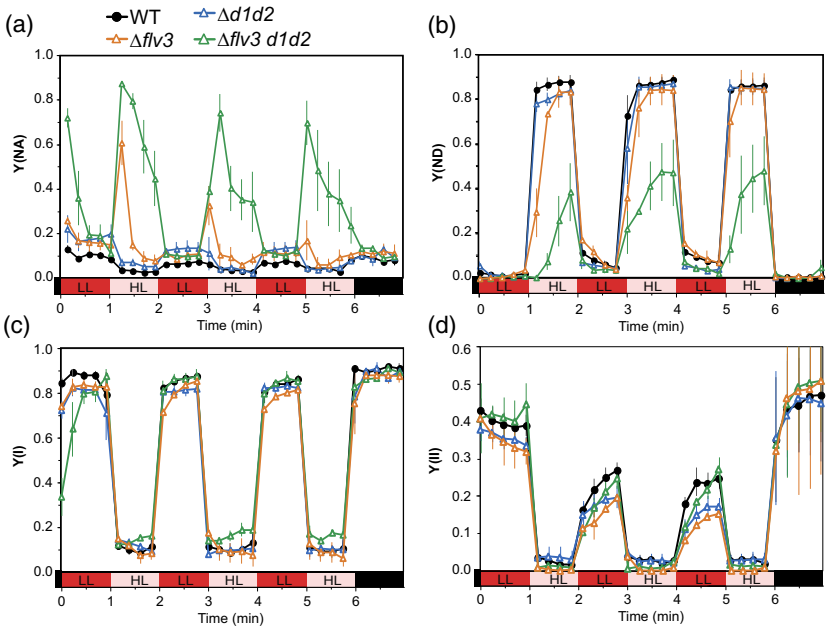

Figure 3. Photosynthetic parameters in wild-type (WT) and mutants strains in fluctuating light intensities.
(a) Acceptor side limitation of photosystem (PS) I, Y (NA), (b) donor side limitation of PSI, Y(ND), as well as (c) effective yield of PSI, *Y*(I) were calculated from absorbance difference changes at 875–830 nm according to Klughammer and Schreiber (2008). Chlorophyll *a* fluorescence changes were measured simultaneously with PSI redox changes and used to calculate (d) effective yield of PSII. Cells were grown in air [CO_2]/moderate light for 4 days, after which the cells were harvested and chlorophyll *a* concentration adjusted to 10 μg ml^{-1} with fresh BG-11. Cells were dark-adapted for 10 min, and then illuminated with red actinic light intensity alternating between 25 and 530 μmol photons m^{-2} sec^{-1} in 1 min periods. Saturating pulses (500 msec of 5000 μmol photons m^{-2} sec^{-1}) were provided every 15 sec. Values shown are averages from 3–4 independent biological replicates ± SE.

previous studies (Helman *et al.*, 2003; Allahverdiyeva *et al.*, 2013). However, during subsequent 1 min cycles of LL/HL, the ability of Δ*flv3* to oxidize PSI in HL improved, suggesting that cells were able to acclimate to the fluctuating light condition via a compensatory mechanism that is distinct from Flv1/3 hetero-oligomers, such as, for example, NDH-1 mediated electron transport.

We detected no acceptor-side limitation during the HL phases in Δ*d1d2* (Figure 3a) as PSI was oxidized similarly to the WT (Figure 3b). However, interestingly, Δ*d1d2* cells exhibited slightly elevated acceptor-side limitation during the LL phases of the experiment (Figure 3a), suggesting a role for NDH-$1_{1,2}$ in maintaining photosynthetic redox poise in light-limited conditions. In the triple mutant strain Δ*flv3 d1d2*, transitions from LL to HL as well as from dark to light caused severe limitation on the acceptor side of PSI, resulting in an inability to oxidize PSI during periodic 1-min HL illumination. Unlike the Δ*flv3* mutant, Δ*flv3 d1d2* did not show improvement in the PSI acceptor side limitation during subsequent cycles. This implies a compensating activity of NDH-1 in Δ*flv3* mutant under the studied conditions. Interestingly, diminished donor side limitation in Δ*flv3 d1d2* resulted in slightly elevated effective yield of PSI during the HL phases (Figure 3c). This could indicate the attenuation of pH-dependent limitation of electron transfer at Cyt b_6f, due to impairment of proton motive force (*pmf*) generation in CET and the Mehler-like reaction. The effective yield of PSII was slightly decreased in HL in Δ*flv3* and Δ*d1d2*, but not in Δ*flv3 d1d2* (Figure 3d).

The differences in photosynthetic electron transport reported above may also be contingent on altered redox states of the NADP+/NADPH pool. Therefore, to investigate the effect of Flv3 and/or NDH-$1_{1,2}$ deficiency on NADP+/NADPH redox kinetics, we recorded NADPH fluorescence changes from dark-adapted cells simultaneously with Chl *a* fluorescence in conditions where actinic light intensity fluctuated between 25 (LL) and 530 μmol photons m^{-2} sec^{-1} (HL) similarly to Figure 3. Upon dark-to-LL transitions, NADPH rapidly accumulated close to a maximal amount in WT, Δ*flv3* and Δ*d1d2* cells, while in Δ*flv3d1d2* the NADP pool was highly reduced already in darkness. Reoxidation of NADPH then occurred in WT and Δ*flv3d1d2* cells, while in Δ*flv3* a slower oxidation phase preceded a transient re-reduction phase during the first minute of illumination (Figure 4a,b). Strong reduction of the NADP+ pool was also detected in Δ*flv3* during the second HL phase of the experiment. In Δ*d1d2* cells, very little oxidation of the NADPH pool occurred during illumination, even at HL–LL transitions (Figure 4c). Chl *a* fluorescence also remained at an elevated level (Figure 4c), suggesting a reduced PQ pool. This was possibly due to delayed activation of CO_2 fixation in the CBB cycle (Figure 2c), and impaired CET or dark respiration. In contrast, NADPH was strongly oxidized in Δ*flv3 d1d2* cells at HL–LL transitions (Figure 4d), but was predominantly reduced in dark-adapted cells (Figure 4d). Upon cessation of illumination, oxidation of the NADPH pool was followed by transient re-reduction after approximately 10 sec. As observed previously (Schreiber and Klughammer, 2009; Holland *et al.*, 2015), the re-reduction peak coincided with a secondary post-illumination rise in Chl *a* fluorescence (PIFR), while oxidation of NADPH paralleled an initial PIFR. The post-illumination re-reduction of NADP+ was diminished and both Chl *a* PIFR peaks were missing in Δ*d1d2* (Figure 4c). Therefore, the PIFR peaks

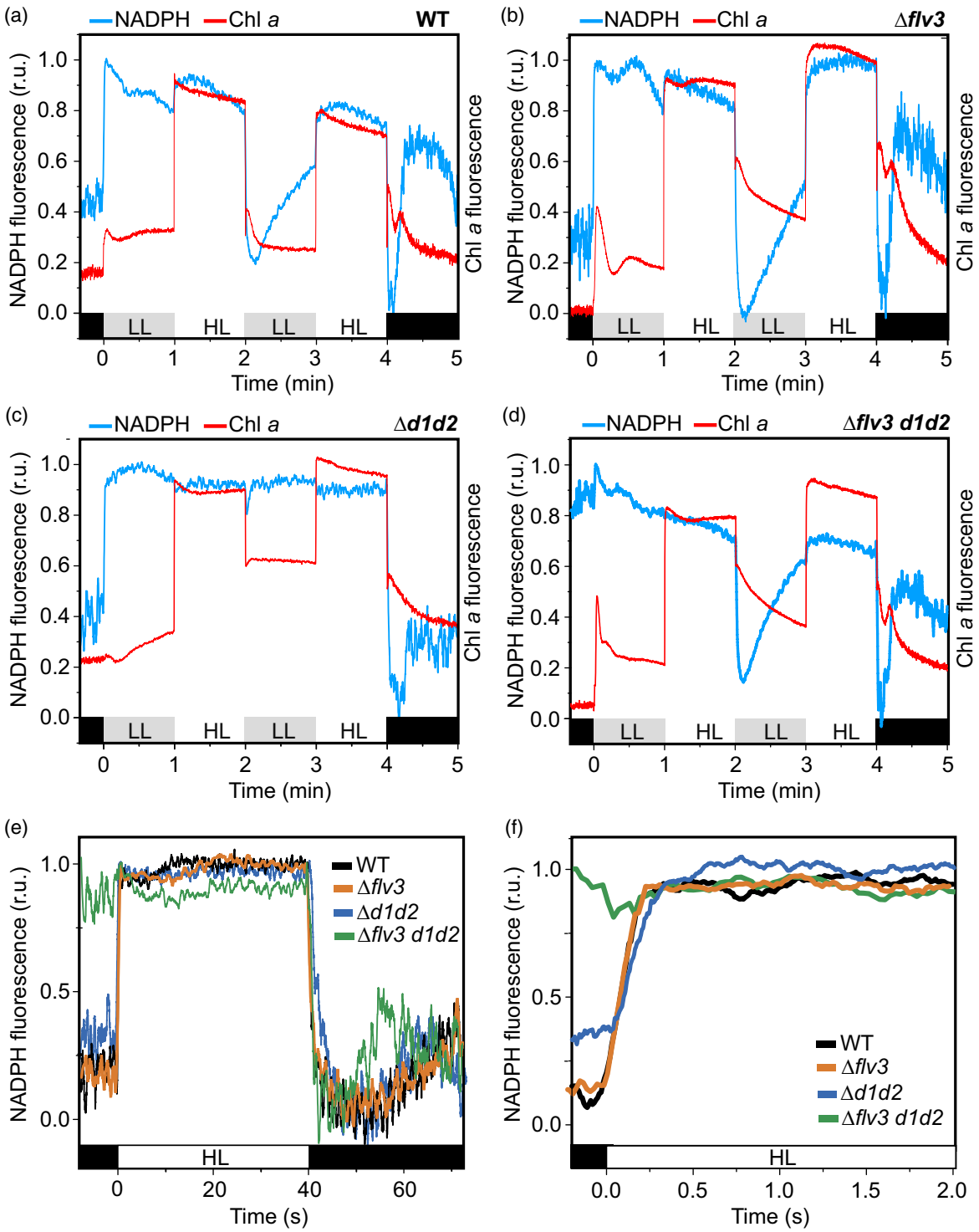

Figure 4. NADPH and chlorophyll (Chl) *a* fluorescence under fluctuating light in wild-type (WT) and mutant strains.
(a) WT, (b) Δ*flv3*, (c) Δ*d1d2*, and (d) Δ*flv3 d1d2* cells were grown in air [CO_2]/moderate light for 4 days, after which the cells were harvested and Chl *a* concentration adjusted to 5 μg ml^{-1} with fresh BG-11. Cells were dark-adapted for 20 min, and then subjected to illumination with red actinic light alternating between 25 and 530 μmol photons m^{-2} sec^{-1} in 1-min periods. NADPH redox changes were monitored with the Dual-PAM 100 spectrophotometer and its 9-AA/NADPH accessory module by measuring fluorescence changes between 420 and 580 nm induced by excitation at 365 nm, as described by (Schreiber and Klughammer, 2009) and (Kauny and Setif, 2014). Chl *a* fluorescence was recorded simultaneously.
(e) NADPH redox changes during illumination of dark-adapted cells with 530 μmol photons m^{-2} sec^{-1}. Other experimental details are as in a–d.
(f) Shows a magnification of the first 2 sec of illumination in (e). Values are normalized according to minimum and maximum fluorescence changes at the onset and cessation of illumination, respectively. Experiments were repeated with three independent biological replicates, of which representative measurements are shown. HL, high light/irradiance; LL, low light/irradiance; r.u., relative units.

probably originate from cyclic and respiratory electron transport via NDH-$1_{1,2}$ (Holland *et al.*, 2015). However, both Chl PIFR peaks were observed in Δ*flv3 d1d2* cells, indicating involvement of a complementary pathway, possibly via succinate dehydrogenase (Cooley and Vermaas, 2001), or a CET pathway dependent on PGR5 and PGRL1-like (Yeremenko *et al.*, 2005; Dann and Leister, 2019). Finally, we monitored NADPH redox kinetics under conditions mimicking the MIMS experiments, where strong O_2 photoreduction occurs in WT and Δ*d1d2* during the first minute of dark-to-high light transition (Figure 2). No substantial differences were observed between the strains, as close to maximal reduction of NADP+ was obtained within approximately 0.25 sec (Figure 4f) and maintained throughout a 40-sec illumination period (Figure 4e). This argues against NADPH being a primary electron donor to either Flv1/3 or NDH-$1_{1,2}$, at least during fast time scales, although based on the current data, we cannot exclude the possibility of NADPH contribution during longer time scales or in steady-state conditions.

Redox status of PSI donor and acceptor side electron carriers and build-up of *pmf* during dark-to-light transitions depend on both Flv1/3 and NDH-$1_{1,2}$

To elucidate the molecular mechanism behind the photosynthetic phenotypes of the studied mutant strains, we next utilized a DUAL-KLAS-NIR spectrophotometer to distinguish between redox changes of plastocyanin (PC), P700 and Fd (Klughammer and Schreiber, 2016; Schreiber, 2017; Setif *et al.*, 2019) upon exposure of dark-adapted cells to HL (503 μmol photons m^{-2} sec^{-1}). Upon illumination of WT cells, rapid oxidation of P700 and PC occurred, followed by transient reduction of PC, P700, as well as Fd after approximately 0.2 sec (Figure 5a). Reoxidation of all three electron carriers then ensued after approximately 0.5 sec. In Δ*flv3* cells, P700 and PC remained mostly reduced after the initial oxidation transient until approximately 3 sec, when another transient and partial reoxidation peak of P700 and PC occurred at approximately 8 sec (Figure 5b). This was followed by re-reduction of P700, similar to that observed recently by Bulychev *et al.* (2018). After 15 sec in light, P700 and PC became gradually oxidized. In contrast to WT, Fd remained reduced for several seconds in light, and was only slowly reoxidized over the 30 sec illumination period (Figure 5b). These observations indicate the importance of Flv1/3 as an electron sink to O_2, accepting electrons presumably from reduced Fd (after approximately 0.5 sec in light). In Δ*d1d2*, redox changes of PC, P700 and Fd were similar to WT, except that the reduction of P700+ following initial oxidation as well as reduction of Fd occurred already after approximately 50 msec (Figure 5c). In Δ*flv3 d1d2*, re-reduction of P700+ and reduction of Fd also occurred already after approximately 50 msec (Figure 5d), suggesting involvement of NDH-$1_{1,2}$ as an acceptor of electrons from Fd at that stage. Fd was reduced more quickly in Δ*flv3 d1d2* than in any other strains and was slowly reoxidized over 30 sec (Figure 5d), probably due to the shortage of electron acceptors (Figure 3a). In summary, these NIR-spectroscopic measurements revealed that Flv1/3 and NDH-$1_{1,2}$ control the redox poise between PSI, PC and primary electron acceptor Fd during specific time frames at transitions to HL. The results are congruent with Fd functioning as the electron donor to both NDH-$1_{1,2}$ and Flv1/3.

To inspect whether the phenotypes observed above depend on differential build-up or regulation of *pmf*, we measured *in vivo* changes in the *pmf* by monitoring the absorbance change difference between 500 and 480 nm, which constitutes the electrochromic shift (ECS) in *Synechocystis* (Viola *et al.*, 2019). *In vivo* measurement of light-induced ECS revealed that after 1 sec of illumination of dark-adapted WT cells with 500 μmol photons m^{-2} sec^{-1}, high *pmf* level was transiently generated, followed by decline during the subsequent seconds (Figure 5e). After approximately 10 sec of illumination, *pmf* again increased towards a steadier value (Figure 5e). Congruently with the strong reduction of P700 and Fd (Figure 5b), the initial *pmf* peak after the first second of illumination was heavily dependent on the presence of Flv1/3. In both Δ*flv3* and Δ*flv3 d1d2*, *pmf* and thylakoid proton flux (vH+) were lower than in WT after 1 sec (Figure 5g). In Δ*flv3*, *pmf* remained drastically lower than in WT during the first seconds of illumination, but differed only slightly from WT thereafter due to diminished conductivity of the thylakoid membrane (gH+) (Figure 5f), which is mainly determined by the activity of the adenosine triphosphate (ATP) synthase (Cruz *et al.*, 2005; Viola *et al.*, 2019). In Δ*d1d2*, the thylakoid proton flux was similar to WT (Figure 5g), probably due to enhanced FDP activity (Figure 2c) compensating for impaired CET and respiration. However, *pmf* remained lower than in WT throughout the 1-min experiment (Figure 5e) because of elevated conductivity (Figure 5f). In contrast, despite drastically lower proton flux (Figure 5g), Δ*flv3 d1d2* cells maintained *pmf* close to the WT levels after the first seconds in light (Figure 5e) due to diminished conductivity (Figure 5f). This indicates that the increased acceptor side limitation of PSI in Δ*flv3 d1d2* in comparison with Δ*flv3* (Figure 3a) is not caused by lack of photosynthetic control as a consequence of lowered *pmf* generation in CET. Based on the comparison of ECS kinetics in single, double and triple mutant cells studied here, we conclude that both Flv1/3 and NDH-$1_{1,2}$ contribute to proton flux during transitions from dark to HL. However, deficiency in NDH-$1_{1,2}$ in Δ*d1d2* is mostly compensated by elevated FDP activity in terms of proton flux, while ATP synthase activity is increased, possibly as a response to the delay in activation of carbon fixation (Figure 2c). In contrast, impaired thylakoid proton flux in Δ*flv3* during

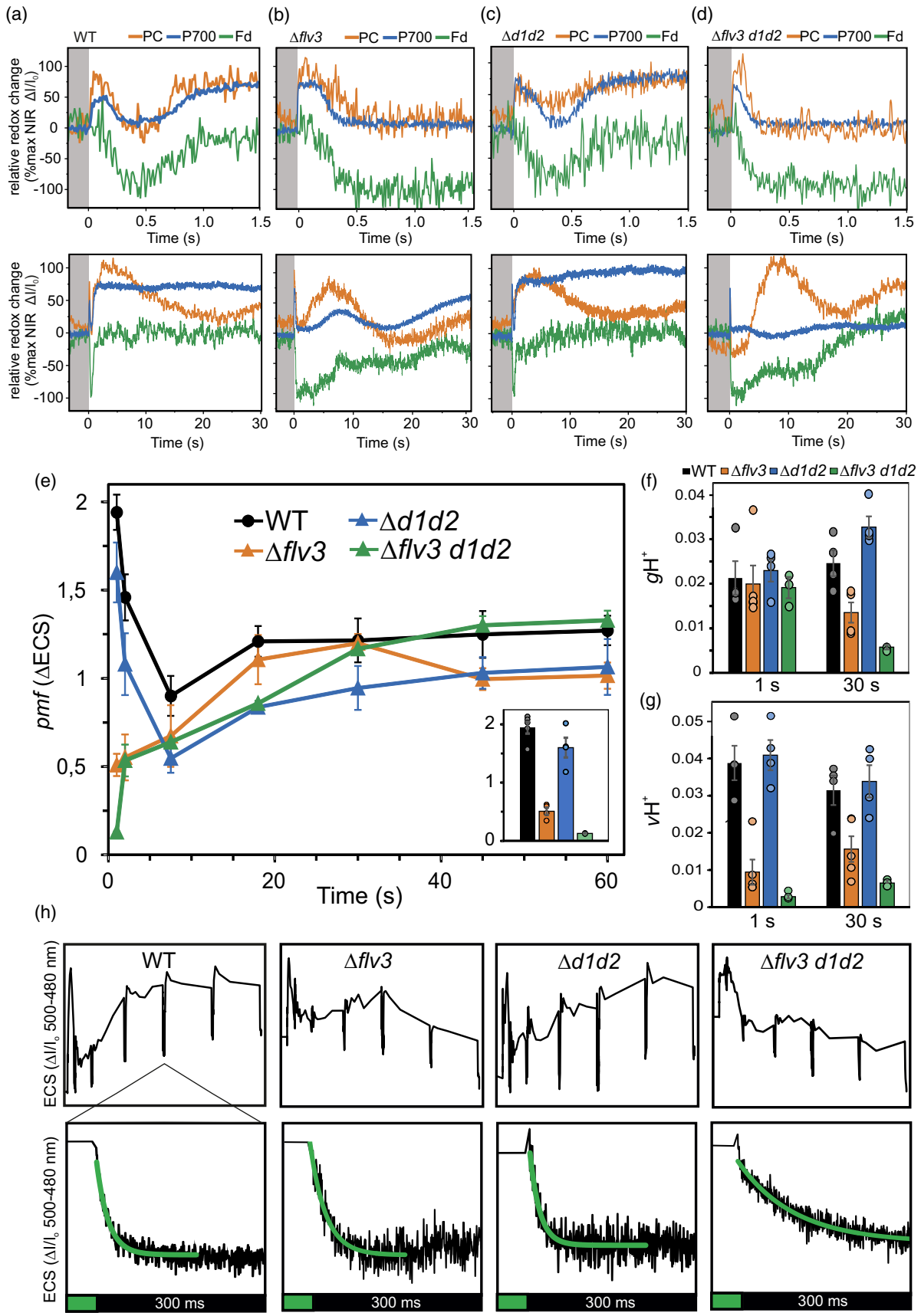

Figure 5. Redox changes of plastocyanin (PC), P700 and ferredoxin (Fd), and build-up of *pmf* during dark-to-high irradiance transitions.
(a) WT, (b) Δ*flv3*, (c) Δ*d1d2*, and (d) Δ*flv3 d1d2* cells were dark-adapted for 10 min, after which absorbance difference changes at 780–820 nm, 820–870 nm, 840–965 nm and 870–965 nm were measured with the DUAL-KLAS-NIR spectrometer during a 30-sec illumination at 503 μmol photons m^{-2} sec^{-1} of red actinic light. PC, P700 and Fd signals were deconvoluted from the absorbance difference changes using differential model plots determined for this study (Figure S3a). Traces were then normalized according to the maximal redox changes determined with the NIRMAX script (Figure S3b) to obtain relative redox changes of PC, P700 and Fd. Upper panels in a–d show magnifications of the first 1.5 sec of illumination from the lower panels. The experiment was repeated with three independent biological replicates, of which representative traces are shown.
(e) Build-up of *pmf* during transitions from dark to 500 μmol photons m^{-2} sec^{-1} of green actinic light. Absorbance difference between 500 and 480 nm (electrochromic shift, ECS) was measured with a JTS-10 spectrometer, and light-induced *pmf* was determined from the dark interval relaxation kinetics of the ECS signal. Means ± SEM from three to four independent experiments are shown. Small inset shows *pmf* values after 1 sec of illumination for a clearer view.
(f) Conductivity of the thylakoid membrane (gH+) after 1 and 30 sec of illumination as in (e). gH+ was determined as the inverse of the time constant of first-order post-illumination decay kinetics of the ECS signal.
(g) Thylakoid proton flux (vH+), calculated as *pmf* × gH+. Individual data points are shown as colored circles in e–g.
(h) Representative traces of 500–480 nm absorbance differences used to determine the values in (e) and post-illumination ECS decay kinetics during a 500 msec dark interval after 30 sec in light (lower panels). First-order fits are shown in green. Cells, after growth in air [CO_2]/50 μmol photons m^{-2} sec^{-1} for 4 days, were harvested and Chl *a* concentration adjusted to 10 μg ml^{-1} with fresh BG-11 for a–d and to 7.5 μg ml^{-1} for e–h.

dark-to-light transitions cannot be compensated by NDH-1. Instead, downregulation of ATP-synthase activity lowers thylakoid conductivity and allows maintenance of *pmf* (apart from the first seconds of illumination) in Δ*flv3* and, even more dramatically, in Δ*flv3 d1d2*.

PSI content is diminished in triple mutants deficient in Flv1/3 and NDH-$1_{1,2}$ shifted to air [CO_2] and HL

The results from the growth assays, along with the real-time gas exchange, P700 redox change and ECS measurements suggested that in Δ*d1d2* cells, an increase in the activity of FDPs compensates for the absence of a functional NDH-$1_{1,2}$ complex, allowing efficient oxidation of PSI under HL. Conversely, in Δ*flv1* and Δ*flv3* mutants, over-reduction of the electron transport chain occurs initially upon exposure to HL, but another mechanism(s) eventually allow acclimation and survival in high [CO_2] and high light (Helman *et al.*, 2003). Under air [CO_2] Flv1/3, hetero-oligomers catalyze transient O_2 photoreduction, which is why no strong growth phenotype is observed in Δ*flv1* or Δ*flv3* under constant HL (Allahverdiyeva *et al.*, 2013; Santana-Sanchez *et al.*, 2019). However, when both Flv1/3 and NDH-$1_{1,2}$ are absent and the electron sink capacity of the cytosol is not elevated by high [CO_2], cells are unable to oxidize PSI in high light, possibly resulting in lethal photodamage to PSI. To assess this hypothesis, we employed immunoblotting to provide estimates of the protein content of PSII (D1) and PSI (PsaB) subunits, orange carotenoid protein (OCP), large isoform of the Fd-NADP+ oxidoreductase (FNR_L), FDPs, as well as NdhD3 and the bicarbonate transporter SbtA after 24 h exposure to different growth conditions.

WT and Δ*flv1* or Δ*flv3* cells grown at 3% [CO_2]/ML and shifted to air [CO_2]/ML at OD = 0.1, accumulated similar levels of the PSII reaction center protein D1 and the PSI subunit PsaB. However, we detected a moderate decrease in the amount of both D1 and PsaB in the Δ*flv1 d1d2* and Δ*flv3 d1d2* triple mutants, while an increased amount of both proteins was detected in Δ*d1d2* (Figure 6a). After 24 h exposure to air [CO_2]/HL, PsaB amount had decreased even further in Δ*flv1 d1d2* and Δ*flv3 d1d2* (Figure 6c). Furthermore, 77K fluorescence spectra revealed that while Δ*flv3 d1d2* and WT cells grown under air [CO_2]/ML had similar PSI/PSII ratios (Figure 6d), the 24-h exposure to air [CO_2]/HL caused a dramatic decrease in the relative PSI fluorescence cross-section (Figure 6e). This strongly supports the hypothesis that loss of PSI contributes to the lethality of the shift to air [CO_2]/HL. Interestingly, a substantial decrease in D1 content in air [CO_2]/HL was also observed in the triple mutants (Figure 6b,c).

Importantly, the Δ*flv1 d1d2* and Δ*flv3 d1d2* strains were unable to induce substantial accumulation of the proteins encoded by the *flv4-2* operon after a shift from 3% to air [CO_2] (Figure 6a,c). Only when pre-grown for 4 days in air [CO_2]/ML before being shifted to higher irradiance, the expression of the operon was induced (Figure 6b). Similar to *flv4-2* operon proteins, both NdhD3 and SbtA failed to accumulate after shifts from 3% to air [CO_2]/HL in the triple mutants, which probably impairs CCM and contributes to the lethal phenotype of the triple mutants in those conditions. Only small amounts of NdhD3 and SbtA were detected also in triple mutant cells shifted from 3% [CO_2] to air [CO_2]/ML (Figure 6a). However, while closer to the WT amount of NdhD3, only a small amount of SbtA was detected after 24 h in air [CO_2]/HL (shifted from air [CO_2]/ML) (Figure 6b). In the Δ*d1d2* mutant, the NdhD3 content was similar to WT, but Flv3 as well as the *flv4-2* operon proteins (Flv2, Flv4 and Sll0218) were upregulated in all conditions tested (Figure 6), which probably contributes to the increased rate of O_2 photoreduction in that strain (Figure 2c). The amounts of OCP and of FNR_L were unchanged in the mutant strains in all conditions (Figure 6).

DISCUSSION

Flv1/3 hetero-oligomers have been shown to be essential for photoreduction of O_2 as a rapid response to excessive reduction of PSI, and consequently, for cell survival under

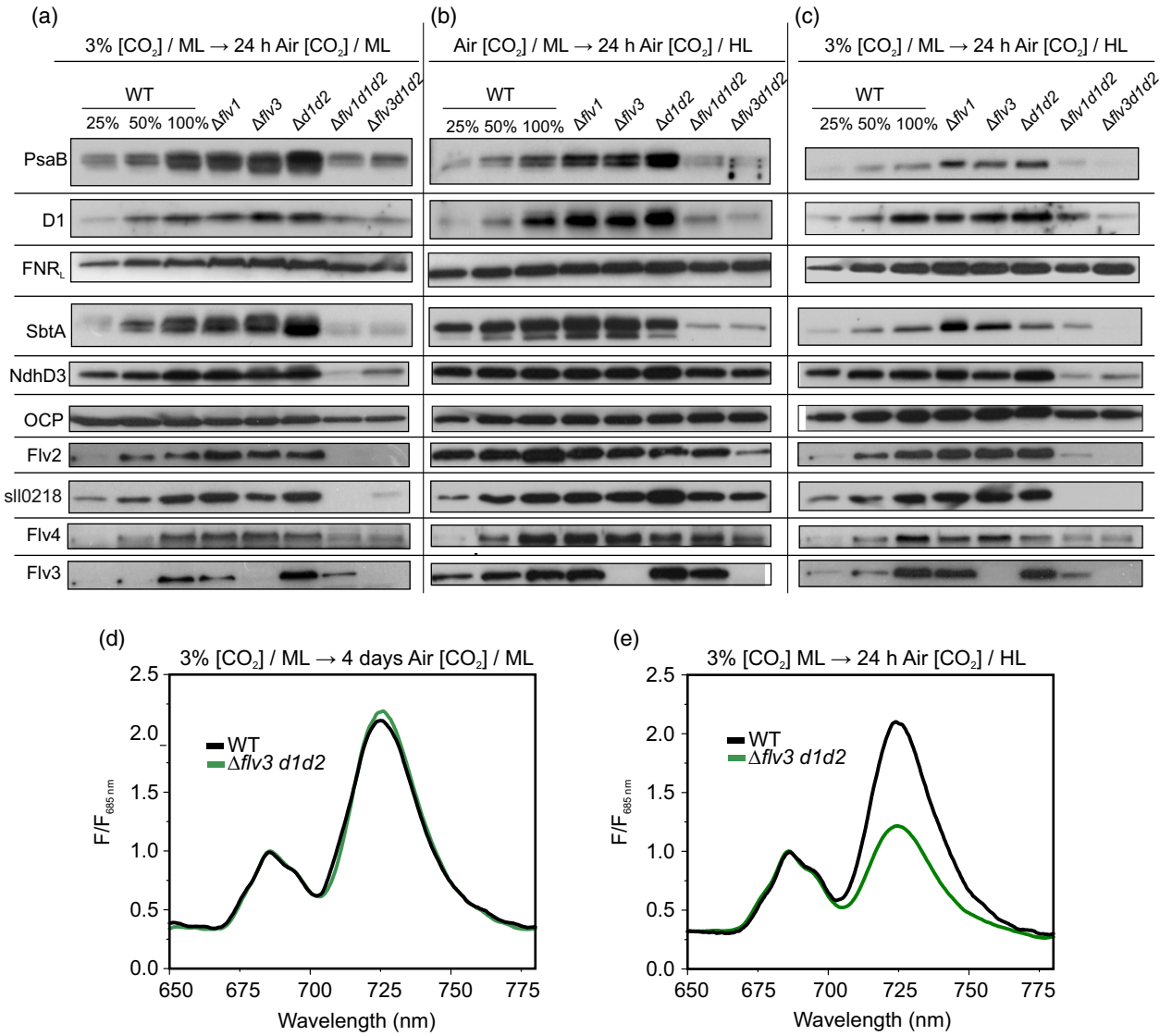

Figure 6. Immunodetection of proteins related to photosynthesis and carbon concentrating mechanism and 77K fluorescence emission spectra in wild-type (WT) and mutant strains.

Pre-cultures were grown for 3 days at 3% [CO_2]/moderate light (ML) (50 μmol photons m^{-2} sec^{-1}) and then pelleted, resuspended in fresh BG-11 at OD_{750} = 0.15 and (a) incubated for 24 h in air [CO_2]/ML, (b) grown for 4 days in air [CO_2]/ML, harvested, resuspended in BG-11 at OD_{750} = 0.15 and then incubated for 24 h in air [CO_2]/HL (220 μmol photons m^{-2} sec^{-1}), (c) incubated for 24 h in air [CO_2]/high light (HL). Total protein extracts were separated by sodium dodecyl sulfate–polyacrylamide gel electrophoresis and probed with specific antibodies. Immunoblots shown are representative of two to three independent biological replicates.

(d) 77K fluorescence emission spectra from intact WT and Δ*flv3 d1d2* cells grown for 4 days in air [CO_2]/ML.

(e) After pre-growth at 3% [CO_2]/ML cells were pelleted, resuspended in fresh BG-11 at OD_{750} = 0.15 and incubated for 24 h in air [CO_2]/HL. Cells (d and e) were pelleted, adjusted to [chlorophyll *a*] of 7.5 μg ml^{-1}, and excited with 440 nm light at 77K. Spectra were normalized to the PSII fluorescence peak at 685 nm.

fluctuating light conditions (Allahverdiyeva *et al.*, 2013; Santana-Sanchez *et al.*, 2019). Moreover, we recently showed that in air [CO_2], Flv2/4 hetero-oligomers also catalyze low-level light-induced steady-state reduction of O_2 on the acceptor side of PSI in a coordinated manner with Flv1/3 (Santana-Sanchez *et al.*, 2019).

Another alternative electron transport component, the NDH-1 complex, in turn, functions in CET around PSI, using Fd as the electron donor (Saura and Kaila, 2019; Schuller *et al.*, 2019). Besides CET, the NDH-$1_{1,2}$ complexes, incorporating the NdhD1 or NdhD2 subunit, are involved in respiration, whereas NDH-$1_{3,4}$ complexes, incorporating the NdhD3 or NdhD4 subunit, function in CO_2 uptake. In the current study, we have used *Synechocystis* mutant strains with different combinations of deficiencies in Flv1/3 and NDH-1 to examine the

physiological significance of these alternative electron transport pathways and the possibility of functional interdependence between them. Our results provide compelling evidence for the concomitant physiological functions of Flv1/3 and NDH-$1_{1,2}$ and their dynamic coordination for the efficient oxidation of PSI (thus protecting it from photodamage) under variable light conditions, and when low [CO_2] limits the consumption of reductants in the CBB cycle. The two pathways can compensate for each other's absence to some extent, but absence of both the Flv1/3 hetero-oligomer and NDH-$1_{1,2}$ is lethal when cells are transferred from elevated [CO_2] to the combined condition of air level [CO_2] and HL (Figure 1d,e). In addition to the absence of these two important pathways, lethality is due to an inability to accumulate low C_i-inducible photoprotective CCM proteins (Figure 6c). Combined deficiency of Flv1/3 and NDH-$1_{3,4}$ did not result in a lethal phenotype upon similar shifts, indicating that functional redundancy exists specifically between the Mehler-like reaction and NDH-$1_{1,2}$

Coordinated functions of Flv1/3 and NDH-$1_{1,2}$ protect PSI by maintaining redox poise between the PETC and carbon fixation

Cells lacking functional Flv1/3 hetero-oligomers suffer from transient over-reduction of PSI during sudden increases in light intensity (Figures 3 and 5) due to the impairment of the Mehler-like reaction (Figure 2; Allahverdiyeva *et al.*, 2013). Whilst NAD(P)H has been proposed as the electron donor to Flv3 (Vicente *et al.*, 2002; Brown *et al.*, 2019) and Flv1 homo-oligomers (Brown *et al.*, 2019), *in vivo* experiments have been unsupportive (Mustila *et al.*, 2016), with exact electron donor(s) to FDP hetero-oligomers yet to be proven. *In vivo* experiments performed in this study demonstrate that the quick reoxidation of Fd after 0.5 sec (Figure 5a) in light is absent in the Δ*flv3* deletion strains, whereby Fd remains strongly reduced (Figure 5b). This result, together with the lack of impairment in $NADP^+$ reduction and oxidation kinetics of Δ*flv3* deletion strains (similar conditions, Figure 4f) provide strong support for Fd, rather than NAD(P)H, being the primary electron donor to the Flv1/3 hetero-oligomer *in vivo*. Accordingly, Fd has been shown to interact with Flv1 and Flv3 by Fd chromatography (Hanke *et al.*, 2011) and with Flv3 using a two-hybrid assay (Cassier-Chauvat and Chauvat, 2014).

The deficiency of NDH-$1_{1,2}$, in turn, reduced the ability of cells to maintain oxidized P700 and Fd under HL soon after (approximately 50–200 msec) a dark-to-light transition (Figure 5c). This brief time scale may be due to PSI-NDH-1 supercomplexes (Gao *et al.*, 2016) where P700 can be oxidized rapidly upon the onset of illumination. It has been shown that formation of the NDH-1-PSI supercomplex is important to keep PSI functional under various stress conditions (Zhao *et al.*, 2017). NDH-$1_{1,2}$ deficiency also caused slightly elevated acceptor side limitation of PSI under LL (Figure 3a), which was probably due to a lack of NADPH oxidation during the low light phases of fluctuating light (Figure 4c). Thus, NDH-$1_{1,2}$ appears to play an important role under low light, as has been previously suggested for chloroplastic NDH in angiosperms (Yamori *et al.*, 2011; Yamori *et al.*, 2015) and bryophytes (Ueda *et al.*, 2012). The delayed activation of CBB in Δ*d1d2* did not result in an inability to oxidize PSI (Figures 3b and 5c), probably due to significant enhancement of FDP-mediated O_2 photoreduction (Figure 2c) providing an enlarged electron sink for the PETC. An opposite order of causation is also possible, whereby the excessive funneling of photosynthetic electrons to O_2 would cause the delay in induction of CO_2 fixation in Δ*d1d2*. However, the observation that there is no NADPH shortage at the onset of illumination in Δ*d1d2,* and rather the consumption of NADPH during transitions from HL to LL is impaired (Figure 4c), suggests that the availability of reductant for the CBB cycle is not the limiting factor. Nor is it probably CO_2, as CCM is functioning as in WT (Figure 2c), or ATP, as ATP synthase activity was even higher than in WT in Δ*d1d2* (Figure 5f). One possibility is that the increased funneling of electrons from Fd to the Mehler-like reaction in Δ*d1d2* (Figure 2c), while not impairing FNR function (and thus NADPH production), might cause a shortage of electrons for the ferredoxin–thioredoxin reductase. This would impair light-dependent activation of the CBB cycle by the thioredoxin system (Michelet *et al.*, 2013; Guo *et al.*, 2014). In addition, it might explain the delay observed in CO_2 fixation in Δ*d1d2*. Nevertheless, simultaneous deficiency of FDPs in addition to NDH-$1_{1,2}$ (in Δ*flv3 d1d2* triple mutant), with the effect of diminishing the flow of photosynthetic electrons to O_2 photoreduction, mostly rescued the delay in CO_2 fixation (Figure 2d) as well as NADPH consumption (Figure 4d) seen in Δ*d1d2*. Transient O_2 photoreduction at a low rate was still observed in Δ*flv3 d1d2* during dark-to-HL transitions (Figure 2d), possibly mediated by the thylakoid terminal oxidases (Ermakova *et al.*, 2016) or by photorespiration (Allahverdiyeva *et al.*, 2011). However, the triple mutants have more severe inability to oxidize PSI than Δ*flv3* during sudden increases in irradiance (Figure 3). These observations suggest that, in addition, Flv1/3 and NDH-$1_{1,2}$ have a role in contributing to oxidation of PSI during changes in light conditions or carbon availability. Upon deficiency of NDH-$1_{1,2}$ (in Δ*d1d2*), cells prioritize the protection of PSI over efficient CO_2 fixation by upregulating the Mehler-like reaction via an unknown mechanism. The triple mutants cannot do this, leading to the timely induction of CO_2 fixation at the high cost of inability to oxidize PSI (Figure 3a) or Fd (Figure 5d). This results in loss of PSI (Figure 6), possibly due to photodamage to its FeS clusters (Tiwari *et al.*, 2016; Shimakawa *et al.*, 2016).

On the mechanism of NDH-1-mediated oxidation of PSI

The contribution of NDH-1 to oxidation of PSI during sudden increases in light intensity is not unprecedented. In angiosperms, where FDPs have been lost during evolution (Ilik *et al.*, 2017), Arabidopsis mutants lacking the NDH complex show a delay in oxidation of PSI during increases in light intensity in comparison with Arabidopsis WT (Nikkanen *et al.*, 2018; Shimakawa and Miyake, 2018a). By definition, canonical CET cannot directly increase the relative proportion of oxidized P700, as electrons from the acceptor side of PSI are shunted back to the intersystem electron transfer chain. However, NDH-1 may enhance PSI oxidation by at least three alternative, but mutually non-exclusive mechanisms.

i NDH-1-mediated CET is coupled to the translocation of protons from cytosol to the thylakoid lumen with a $2H^+/e^-$ stoichiometry (Strand *et al.*, 2017; Saura and Kaila, 2019). Therefore, it will contribute to build-up of ΔpH, which limits electron transfer to PSI by inhibiting PQH_2 oxidation at Cyt *b6f* (Shimakawa and Miyake, 2018b) and drives ATP synthesis to accommodate the needs of the CBB, increasing its electron sink capacity. As the Mehler-like reaction also contributes to build-up of ΔpH by consuming H^+ on the cytosolic side of the thylakoid membrane and by supporting linear electron flow (Figure 5), (Allahverdiyeva *et al.*, 2013), enhanced FDP activity in Δ*d1d2* (Figure 2c) partly compensates for the lack of NDH-$1_{1,2}$ in respect to the generation of proton flux (Figure 5g). However, this fails to explain the exacerbated impairment of P700 and Fd oxidation in Δ*flv3 d1d2* in comparison with Δ*flv3* (Figures 3 and 5) because in the triple mutant *pmf* was not lower than in Δ*flv3* (Figure 5e). However, adequate *pmf* is maintained at the expense of ATP synthase activity (Figure 5f), and it is likely that diminished ATP production contributes to the increased acceptor side limitation of PSI in Δ*flv3 d1d2* (Figure 3a). Therefore, NDH-$1_{1,2}$ could contribute to P700 oxidation by enhancing cytosolic sink capacity by providing a more suitable ATP/NADPH ratio for the CBB. Adjustment of the ATP/NADPH ratio closer to the theoretically optimal 3:2 has long been considered a fundamental reason for the existence of CET (Kramer *et al.*, 2004; Yamori and Shikanai, 2016).

ii NDH-1-mediated respiratory electron transfer, that is, coupling of PQ reduction by NDH-1 to O_2 reduction by thylakoid terminal oxidases (i.e. Cyd and Cox), would also contribute to oxidation of PSI by relieving electron pressure in the intersystem chain during illumination (Ermakova *et al.*, 2016), as well as contribute further to ΔpH by consuming H^+ on the cytosolic side of thylakoids (Cyd) and pumping protons to the lumen (Cox) (Brändén *et al.*, 2006). Interestingly, Liu *et al.* (2012) have shown that the subcellular localization of NDH-1 complexes is dependent on the redox state of the PQ pool. An oxidized PQ pool causes NDH-1 to accumulate at specific clusters in thylakoid membranes where it would probably transfer electrons (via the PQ pool) to a terminal oxidase. A reduced PQ pool, in turn, results in a more even distribution of NDH-1 within thylakoids (Liu *et al.*, 2012). However, it is important to note that terminal oxidases do not have a high electron sink capacity (Ermakova *et al.*, 2016).

iii NDH-1 has been predicted, albeit not yet experimentally shown in photosynthetic organisms, to be able to function in reverse: to oxidize PQH_2 driven by concomitant release of protons from the thylakoid lumen (Strand *et al.*, 2017). Such reverse activity would constitute a "pseudo-linear" electron transfer pathway that would bypass PSI and thereby prevent its over-reduction. This could occur in conditions where the PQ pool is reduced, *pmf* is high and the Fd pool is oxidized (Strand *et al.*, 2017). Such conditions probably exist transiently during dark-to-light and LL-to-HL transitions (Figures 4 and 5) (Strand *et al.*, 2019). Accordingly, fast re-reduction of P700+ already after 50 msec was observed in Δ*d1d2* and Δ*flv3 d1d2* during dark-to-HL transitions (Figure 5c). As supported by the impaired ability to oxidize Fd in the absence of Flv1/3 (Figure 5), the presence of the Flv1/3-catalyzed Mehler-like reaction would probably be essential in this model to maintain the Fd pool in a sufficiently oxidized state to provide electron acceptors for reverse-functioning NDH-1. However, it is noteworthy that NDH-1 reverse activity would also have the effect of lowering ΔpH, thereby relieving photosynthetic control at Cyt *b6f*. This could counteract the effect of any reverse NDH-1 activity by increasing electron flow to PSI.

Hypothetical mechanisms for the coordination of Flv1/3 and NDH-$1_{1,2}$ activities are shown in Figure 7.

Inability to induce a strong CCM network contributes to lethality upon shifts to air [CO_2]/HL in cells deficient in both Flv1/3 and NDH-$1_{1,2}$

Exposure of *Synechocystis* cells to low [CO_2] induces expression of high-affinity CCM-related genes such as SbtA, a HCO_3^-/Na^+ symporter on the plasma membrane, and NdhD3, which is part of the NDH-1_3 complex on thylakoids specializing in C_i uptake (Ohkawa *et al.*, 2000b; Shibata *et al.*, 2001; Shibata *et al.*, 2002; Zhang *et al.*, 2004). CCM is energetically expensive, but the large C_i flux involved in the operation of CCM contributes to dissipation of excess light energy under stress conditions (Xu *et al.*, 2008; Burnap *et al.*, 2015). NDH-$1_{3,4}$ in particular has a photoprotective role, using reduced Fd to drive CO_2 conversion to HCO_3^- with concomitant translocation of protons into the thylakoid lumen.

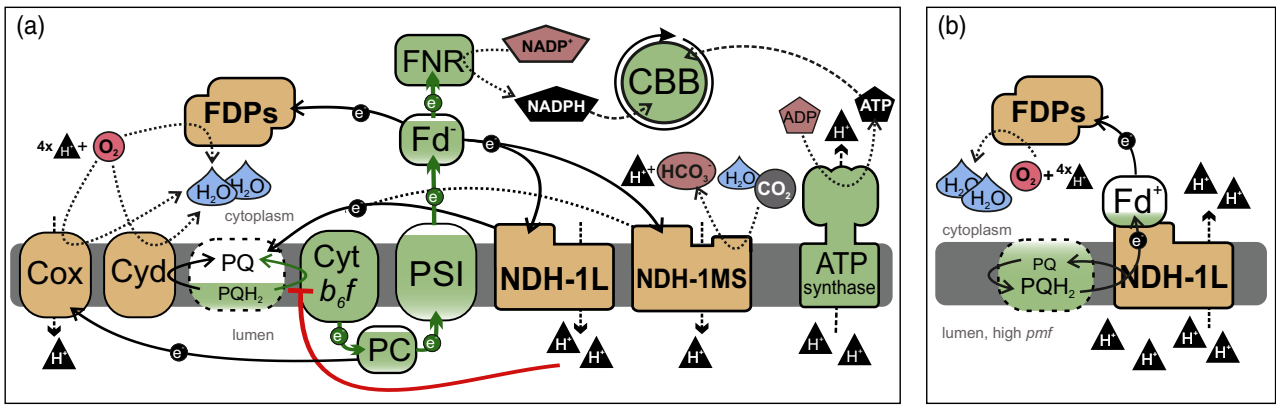

Figure 7. Schematic models for the coordination of the activities of flavodiiron proteins (FDPs) and NDH-1 in preventing over-reduction of photosystem (PS) I.
(a) In conditions where the ferredoxin (Fd) pool is highly reduced and the plastoquinone (PQ) pool is not, NDH-1L transfers electrons from Fd to the PQ pool, coupled to O_2 reduction by thylakoid-localized terminal oxidases (RTOs). NDH-1L pumps $2H^+/e^-$ into the lumen while FDPs and RTOs consume H^+ when reducing O_2 to H_2O on the cytosolic side of thylakoids. This increases transthylakoid *pmf*, which in turn drives adenosine triphosphate (ATP) synthesis as well as inhibits PQH_2 oxidation at Cyt b_6f (depicted by a blunt-ended red curve), thereby preventing excessive electron supply to PSI. Carbonic anhydrase activity of NDH1-MS converts CO_2 to HCO_3^-, consuming H^+ in the cytosol, probably also coupled to translocation of H^+ to the lumen, further increasing *pmf*. Increased availability of CO_2 and ATP/NADPH ratio enhances the electron sink capacity of the Calvin–Benson–Bassham cycle (CBB) on the acceptor side of the photosynthetic electron transport chain.
(b) If the PQ pool is highly reduced, Fd pool is oxidized, and *pmf* is high, NDH-1L could hypothetically function in reverse, transferring electrons from PQH_2 to Fd+, powered by release of $2H^+/e^-$ from the lumen. A strong Mehler-like reaction catalyzed by Flv1/3 would be required to maintain a sufficient pool of oxidized Fd, with Flv1/3 probably accepting electrons directly from Fd–. Most components depicted in (a) are omitted from (b) to enhance clarity, not to suggest their absence. Extent of the color fill for PQ/PQH_2 and Fd depict level of reduction. FNR, ferredoxin-$NADP^+$-reductase; PC, plastocyanin.

Despite the low induction level of the CCM proteins, NdhD3 and SbtA, the triple mutants (Figure 6) survive under standard growth conditions of air [CO_2]/ML (Figure 1b,c), but their growth was retarded on solid media (Figure 1e) The difference may be due to the differential diffusivity of CO_2 in solid media in comparison with suspension cultures (Ohkawa *et al.*, 2000a); that is, the impairment of CCM in the triple mutants becomes more limiting on solid media. However, when a decrease in [CO_2] is coupled with an increase in irradiance a low amount of CCM, reflected by the low accumulation level of NdhD3 and SbtA in the Δ*flv1d1d2* and Δ*flv3d1d2* triple mutants (Figure 6c) fails to dissipate excess energy, thus resulting in photodamage and lethality of those conditions. The regulatory mechanisms controlling the inability of the triple mutants to accumulate low Ci-inducible proteins are unclear and remain to be elucidated. Accumulation of NADP+ and α-ketoglutarate inhibits the induction of CCM gene expression via interaction with the transcription factor NdhR (CcmR) (Daley *et al.*, 2012). NdhR also controls expression of the Flv4-2 operon encoding Flv2, Flv4 and Sll0218 (Eisenhut *et al.*, 2012), all of which also showed decreased accumulation levels in the triple mutants (Figure 6). However, at least in the tested conditions, no substantial increase in the relative amount of NADP+ was detected in Δ*flv3d1d2* cells (Figure 4). Nevertheless, it is important to note that Flv1/3 and NDH-$1_{3,4}$ cooperation alone is not crucial for cell metabolism, as the Δ*flv1 d3d4* and Δ*flv3 d3d4* mutant cells do not show clear growth phenotypes (Figure S1).

Conclusions

In the current study, we have shown that FDPs and NDH-1 function cooperatively to maintain redox balance between the PETC and cytosolic carbon assimilation upon sudden changes in light intensity and/or carbon availability. It is probable that both pathways receive electrons primarily from Fd, which enables coordinated regulation of their activities. Cooperation of FDPs and NDH-1 has an essential photoprotective role during shifts to air [CO_2]/HL, contributing to efficient oxidation of PSI, build-up of *pmf* and induction of expression of low C_i-specific CCM-related genes. A key issue yet to be elucidated is the regulatory mechanism(s) by which the dynamic coordination of FDP and NDH-1 activities is achieved. One potential regulatory mechanism could function through the light-dependent Fd–thioredoxin system, which by competing with FDPs and NDH-1 for electrons from Fd, could constitute an effective regulatory feedback-loop. Indeed, light-dependent redox-sensitive cysteine residues have been identified in Flv1 and Flv3 as well as in several subunits of NDH-1 (Guo *et al.*, 2014), and activity of chloroplastic NDH-1 in plants has been reported to be regulated by thioredoxins (Courteille *et al.*, 2013; Nikkanen *et al.*, 2018).

Finally, it is worth noting that simultaneous removal of Flv1/3 and NDH-$1_{1,2}$ as competitive electron sinks downstream of PSI may be a useful biotechnological tool for maximizing the direction of photosynthetic electrons to desired pathways under controlled environmental conditions (McCormick *et al.*, 2013; Thiel *et al.*, 2019; Jokel *et al.*,

2019). Furthermore, our findings about the functional interplay between FDPs and NDH-1 will be highly relevant in projects aiming to enhance crop productivity via introduction of exogenous FDPs to higher plants (Yamamoto *et al.*, 2016; Gómez *et al.*, 2018).

EXPERIMENTAL PROCEDURES

Strains and culture conditions

In the current study we used the glucose-tolerant WT strain *Synechocystis* sp. PCC 6803 (Williams, 1988), single mutant strains Δ*flv1* and Δ*flv3* (Helman *et al.*, 2003), M55 mutant (Δ*ndhB*) (Ogawa, 1991), double mutants Δ*d1d2 and* Δ*d3d4* (Ohkawa *et al.*, 2000a) and triple mutants Δ*flv1 d1d2,* Δ*flv3 d1d2,* Δ*flv1 d3d4* and Δ*flv3 d3d4* obtained from the CyanoMutants collection (Nakamura *et al.*, 1999). The triple mutants were constructed by T. Ogawa in Δ*d1d2* and Δ*d3d4* backgrounds. All the mutants demonstrated complete segregation in the presence of antibiotic. Pre-experimental cultures were always grown in 30 ml batches of BG-11 medium pH 7.5 (Williams, 1988) under 3% [CO_2] at 30°C under continuous white light of 50 μmol photons m^{-2} sec^{-1} (ML) with agitation. Mutant pre-cultures were supplemented with the appropriate antibiotics. At the logarithmic growth phase, cells were harvested and resuspended in fresh BG-11 without antibiotics at OD_{750} of 0.1–0.2, as described in the appropriate figure legends. Cells were then shifted to air [CO_2]/30°C and illuminated continuously with white light of either 50 or 220 μmol photons m^{-2} sec^{-1}, as described in the figure legends.

Gas exchange measurements

The exchange of $^{16}O_2$ (*m/z* 32), $^{18}O_2$ (*m/z* 36) and CO_2 (*m/z* 44) was measured *in vivo* with MIMS as described in Mustila *et al.* (2016). Harvested cells were resuspended in fresh BG-11 pH 7.5 and adjusted to 10 μg Chl *a* ml^{-1}, and kept for 1 h in air [CO_2]/50 μmol photons m^{-2} sec^{-1}. Before measurements, cells were supplemented with $^{18}O_2$ at an equivalent concentration to $^{16}O_2$ and with 1.5 mM $NaHCO_3$. Cells were dark-adapted for 15 min, after which gas exchange was monitored over a 5-min illumination period of 500 μmol photons m^{-2} sec^{-1} of white actinic light (AL). The gas exchange rates were calculated according to Beckmann *et al.* (2009).

Measurement of fluorescence and absorbance changes

Experimental cultures for all spectroscopic experiments were grown for 4 days in air [CO_2]/50 μmol photons m^{-2} sec^{-1} at 30°C in BG-11 pH 7.5. Chl *a* fluorescence and P700 oxido-reduction (875–830 nm absorbance difference) were simultaneously recorded (Figure 3) with the Dual-PAM 100 spectrophotometer (Walz, Effeltrich, Germany). Harvested cells were resuspended in fresh BG-11 pH 7.5 and adjusted to 10 μg Chl *a* ml^{-1}, and kept for 1 h in air [CO_2]/50 μmol photons m^{-2} sec^{-1} and dark-adapted for 10 min before being subjected to a fluctuating light regime alternating between 1-min periods of 25 and 530 μmol photons m^{-2} sec^{-1} of red AL. Saturating pulses (500 msec of 5000 μmol photons m^{-2} sec^{-1}) were administered at 15 sec intervals. Photosynthetic parameters were calculated as follows: $Y(NA) = (P_m - P_m')/P_m$; $Y(ND) = P/P_m$; $Y(I) = 1 - Y(ND) - Y(NA)$ (Klughammer and Schreiber, 2008); $Y(II) = (F_m' - F)/F_m'$ (Genty *et al.*, 1989).

A DUAL-KLAS-NIR spectrophotometer (Walz) was used to measure absorbance difference changes at 780–820, 820–870, 840–965 and 870–965 nm, from which PC, P700 and Fd redox changes (Figure 5) were deconvoluted based on differential model plots (DMPs) for PC, P700 and Fd (Klughammer and Schreiber, 2016; Schreiber, 2017; Setif *et al.*, 2019). The redox changes were then normalized according to the maximal redox changes determined with the NIRMAX script of the instrument software (Figure S3b), consisting of a 3 sec illumination of red AL (200 μmol photons m^{-2} sec^{-1}), with a saturating pulse after 200 msec of illumination to reduce the Fd pool fully. After 4 sec of darkness thereafter, cells were illuminated under far red light for 10 sec with a saturating pulse administered in the end of the illumination period to oxidize P700 fully. In WT *Synechocystis*, very fast reoxidation of Fd upon illumination impedes the measurement of model spectra. To circumvent this issue, we measured the DMPs from Δ*flv3 d1d2* cells where P700 oxidation was severely delayed in comparison with WT (Figure 3b). The DMPs (Figure S3a) were measured using scripts provided with the instrument software. Harvested cells were adjusted to 10 μg Chl *a* ml^{-1} with fresh BG-11 pH 7.5, and kept for 1 h in air [CO_2]/50 μmol photons m^{-2} sec^{-1} and dark-adapted for 30 min before illumination for 30 sec with 503 μmol photons m^{-2} sec^{-1} of red AL. It is noteworthy that cytochrome c_6 and (F_AF_B) redox changes probably contribute to the PC and Fd signals, respectively (Setif *et al.*, 2019).

NADPH fluorescence changes between 420 and 580 nm, induced by excitation at 365 nm, were measured simultaneously with Chl *a* fluorescence with the Dual-PAM 100 and its 9-AA/NADPH accessory module (Walz) (Schreiber and Klughammer, 2009; Kauny and Setif, 2014). Experimental samples were prepared as above and [Chl *a*] was adjusted to 5 μg ml^{-1}. Cells were dark-adapted for 20 min and subjected to the same fluctuating light regime as in Figure 3, but without saturating pulses.

The ECS was measured as the absorbance difference between 500 and 480 nm (Viola *et al.*, 2019). Absorbance changes were measured from dark-adapted cell suspensions with a JTS-10 spectrophotometer (BioLogic, Seyssinet-Pariset, France) using 500 and 480 nm CWL 50 mm 10 nm FWHM bandpass filters (Edmund Optics, Barrington, NJ, USA) and BG39 filters (Schott, Mainz, Germany) protecting the light detectors from scattering effects. Absorbance changes induced by measuring light only were subtracted from changes under ML + AL. ECS values were normalized to ECS change induced by a single turnover flash provided by an XST-103 xenon lamp (Walz). Experimental samples were prepared as above and [Chl *a*] was adjusted to 7.5 μg ml^{-1}, and illuminated with green AL of 500 μmol photons m^{-2} sec^{-1} for 1 or 60 sec interspersed with 500 msec dark intervals at 2, 7.5, 18, 30 and 45 sec. *Pmf* was calculated as the extent of ECS decrease at the dark intervals. Thylakoid conductivity (gH+) was calculated as the inverse of the time constant of a first-order fit to ECS relaxation kinetics during a dark interval, and proton flux (vH+) as *pmf* × gH+ (Cruz *et al.*, 2005). Representative ECS traces of whole 60 sec measurements (upper panels) as well as fast kinetics during dark intervals after 30 sec illumination (lower panels) from WT, Δ*flv3*, Δ*d1d2* and Δ*flv3 d1d2* cells are shown in Figure 5h.

77K fluorescence emission spectra were measured with a QE Pro spectrophotometer (Ocean Optics, Dunedin, FL, USA). Cells were harvested and [Chl *a*] was adjusted to 7.5 μg ml^{-1} with fresh BG-11 pH 7.5. Cells were frozen in liquid N_2 and excited at 440 nm. Raw spectra were normalized to the PSII-fluorescence peak at 685 nm.

Protein extraction and immunoblotting

Total protein extracts from cultures were isolated as previously described (Zhang *et al.*, 2009), separated by sodium dodecyl sulfate–polyacrylamide gel electrophoresis on 12% gels with 6 M urea

and blotted on polyvinylidene fluoride membranes. Membranes were probed with antibodies raised against D1, PsaB (AS10 695; Agrisera, Vännäs, Sweden), PetH (kindly shared by H. Matthijs), OCP (kindly shared by D. Kirilovsky), SbtA (kindly shared by T. Ogawa), NdhD3 (Eurogentec, Liége, Belgium), Flv2, Flv4 and Flv3 (Antiprot, Puchheim, Germany), and Sll0218 (MedProbe, Oslo, Norway). Horseradish peroxidase-conjugated secondary antibody (GE Healthcare, Chicago, IL, USA) and Amersham ECL (GE Healthcare) were used for detection.

ACKNOWLEDGEMENTS

We thank Prof. Teruo Ogawa for sharing the FDP and NDH-1 mutants and Dr. Henna Mustila for construction of the ΔM55 *flv3* strain. Dr. Duncan Fitzpatrick is thanked for expertise and assistance with MIMS. We also thank Dr. Pierre Setif and Dr. Gert Schansker for their expert advice on measuring the DMPs for the DUAL-KLAS-NIR spectrophotometer, and Prof. Jens Appel for critical reading of the manuscript. This work was supported by the Academy of Finland (project no. 315119 to Y.A. and the Finnish Center of Excellence, project no. 307335), the NordForsk Nordic Center of Excellence 'NordAqua' (no. 82845) and SFB480, Germany.

AUTHOR CONTRIBUTIONS

LN and YA conceptualized the research; LN, ASS, ME and YA designed the research; ME and ASS conducted growth experiments; LN performed MIMS and spectrophotometric experiments; ASS performed immunoblotting; all authors analyzed the data; LN and YA wrote the article with input from ASS and ME.

CONFLICT OF INTEREST

The authors declare no conflict of interest.

DATA AVAILABILITY STATEMENT

All relevant data can be found within the article and its Supporting information.

SUPPORTING INFORMATION

Additional Supporting Information may be found in the online version of this article.

Figure S1. Growth of Δ*flv1 d3d4* and Δ*flv3 d3d4* and creation of M55 *Δflv3* mutant strains.

Figure S2. O_2 and CO_2 fluxes in M55 and in WT at pH 6.

Figure S3. Near-infrared (NIR) differential model plots (DMPs) for deconvolution of PC, P700 and Fd signals with the DUAL-KLAS-NIR 100 spectrometer.

REFERENCES

Alboresi, A., Storti, M., Cendron, L. and Morosinotto, T. (2019) Role and regulation of class-C flavodiiron proteins in photosynthetic organisms. *Biochem. J.* **476**, 2487–2498. https://doi.org/10.1042/BCJ20180648

Allahverdiyeva, Y., Ermakova, M., Eisenhut, M., Zhang, P., Richaud, P., Hagemann, M., Cournac, L. and Aro, E.M. (2011) Interplay between Flavodiiron proteins and photorespiration in synechocystis sp. PCC 6803. *J. Biol. Chem.* **286**, 24007–24014. https://doi.org/10.1074/jbc.M111.223289

Allahverdiyeva, Y., Mustila, H., Ermakova, M., Bersanini, L., Richaud, P., Ajlani, G., Battchikova, N., Cournac, L. and Aro, E.M. (2013) Flavodiiron proteins Flv1 and Flv3 enable cyanobacterial growth and photosynthesis under fluctuating light. *Proc. Natl. Acad. Sci. USA*, **110**, 4111–4116. https://doi.org/10.1073/pnas.1221194110

Allahverdiyeva, Y., Suorsa, M., Tikkanen, M. and Aro, E.M. (2015) Photoprotection of photosystems in fluctuating light intensities. *J. Exp. Bot.* **66**, 2427–2436. https://doi.org/10.1093/jxb/eru463

Battchikova, N., Eisenhut, M., Aro, E.M. (2011) Cyanobacterial NDH-1 complexes: Novel insights and remaining puzzles. *Biochim Biophys Acta*, **1807**(8), 935–944. https://doi.org/10.1016/j.bbabio.2010.10.017

Beckmann, K., Messinger, J., Badger, M.R., Wydrzynski, T. and Hillier, W. (2009) On-line mass spectrometry: membrane inlet sampling. *Photosynth. Res.* **102**(2-3), 511–522. https://doi.org/10.1007/s11120-009-9474-7

Bernat, G., Appel, J., Ogawa, T. and Rögner, M. (2011) Distinct roles of multiple NDH-1 complexes in the cyanobacterial electron transport network as revealed by kinetic analysis of P700(+) reduction in various ndh-deficient mutants of Synechocystis sp. strain PCC6803. *J. Bacteriol.* **193**, 292–295. https://doi.org/10.1128/JB.00984-10

Brändén, G., Gennis, R.B. and Brzezinski, P. (2006) Transmembrane proton translocation by cytochrome c oxidase. *Biochim Biophys Acta*, **1757**, 1052–1063. https://doi.org/10.1016/j.bbabio.2006.05.020

Brown, K.A., Guo, Z., Tokmina-Lukaszewska, M., Scott, L.W., Lubner, C.E., Smolinski, S., Mulder, D.W., Bothner, B. and King, P.W. (2019) The oxygen reduction reaction catalyzed by Synechocystis sp. PCC 6803 flavodiiron proteins. *Sustain Energ. Fuels*, **3**, 3191–3200. https://doi.org/10.1039/c9se00523d

Bulychev, A.A., Cherkashin, A.A., Muronets, E.M. and Elanskaya, I.V. (2018) Photoinduction of electron transport on the acceptor side of PSI in Synechocystis PCC 6803 mutant deficient in flavodiiron proteins Flv1 and Flv3. *Biochim. Biophys. Acta Bioenerg.* **1859**(10), 1086–1095. https://doi.org/10.1016/j.bbabio.2018.06.012

Burnap, R.L., Hagemann, M. and Kaplan, A. (2015) Regulation of CO_2 concentrating mechanism in cyanobacteria. *Life (Basel)*, **5**, 348–371.

Burnap, R.L., Nambudiri, R. and Holland, S. (2013) Regulation of the carbon-concentrating mechanism in the cyanobacterium *Synechocystis* sp PCC6803 in response to changing light intensity and inorganic carbon availability. *Photosynth. Res.* **118**, 115–124. https://doi.org/10.1007/s11120-013-9912-4

Cassier-Chauvat, C. and Chauvat, F. (2014) Function and regulation of ferredoxins in the cyanobacterium, *Synechocystis* PCC6803: recent advances. *Life*, **4**, 666–680.

Chaux, F., Burlacot, A., Mekhalfi, M., Auroy, P., Blangy, S., Richaud, P. and Peltier, G. (2017) Flavodiiron proteins promote fast and transient O-2 photoreduction in Chlamydomonas. *Plant Physiol.* **174**, 1825–1836. https://doi.org/10.1104/pp.17.00421

Cooley, J.W. and Vermaas, W. (2001) Succinate dehydrogenase and other respiratory pathways in thylakoid membranes of Synechocystis sp strain PCC 6803: capacity comparisons and physiological function. *J. Bacteriol.* **183**: 4251–4258. https://doi.org/10.1128/JB.183.14.4251-4258.2001

Courteille, A., Vesa, S., Sanz-Barrio, R., Cazalé, A.-C., Becuwe-Linka, N., Farran, I., Havaux, M., Rey, P. and Rumeau, D. (2013) Thioredoxin m4 controls photosynthetic alternative electron pathways in Arabidopsis. *Plant Physiol.* **161**, 508–520.

Cruz, J.A., Avenson, T.J., Kanazawa, A., Takizawa, K., Edwards, G.E. and Kramer, D.M. (2005) Plasticity in light reactions of photosynthesis for energy production and photoprotection. *J. Exp. Bot.* **56**, 395–406.

Daley, S.M., Kappell, A.D., Carrick, M.J. and Burnap, R.L. (2012) Regulation of the cyanobacterial CO_2-concentrating mechanism involves internal sensing of NADP+ and α-ketoglutarate levels by transcription factor CcmR. *PLoS ONE*, **7**, e41286. https://doi.org/10.1371/journal.pone.0041286

Dann, M. and Leister, D. (2019) Evidence that cyanobacterial Sll1217 functions analogously to PGRL1 in enhancing PGR5-dependent cyclic electron flow. *Nat. Commun.* **10**, 5299. https://doi.org/10.1038/s41467-019-13223-0

Eisenhut, M., Georg, J., Klähn, S., Sakurai, I., Mustila, H., Zhang, P., Hess, W.R. and Aro, E.M. (2012) The antisense RNA As1_flv4 in the Cyanobacterium Synechocystis sp. PCC 6803 prevents premature expression of the flv4-2 operon upon shift in inorganic carbon supply. *J. Biol. Chem.* **287**, 33153–33162.

Ermakova, M., Huokko, T., Richaud, P., Bersanini, L., Howe, C.J., Lea-Smith, D., Peltier, G. and Allahverdiyeva, Y. (2016) Distinguishing the roles of thylakoid respiratory terminal oxidases in the cyanobacterium Synechocystis sp. PCC 6803. *Plant Physiol.* **171**, 1307–1319. https://doi.org/10.1104/pp.16.00479

Gao, F., Zhao, J., Chen, L., Battchikova, N., Ran, Z., Aro, E.-M., Ogawa, T. and Ma, W. (2016) The NDH-1L-PSI supercomplex Is important for efficient cyclic electron transport in cyanobacteria. *Plant Physiol.* **172**(3), 1451–1464. https://doi.org/10.1104/pp.16.00585

Genty, B., Briantais, J.M. and Baker, N.R. (1989) The relationship between the quantum yield of photosynthetic electron transport and quenching of chlorophyll fluorescence. *Biochim. Biophys. Acta*, **990**(1), 87–92. https://doi.org/10.1016/S0304-4165(89)80016-9

Gerotto, C., Alboresi, A., Meneghesso, A., Jokel, M., Suorsa, M., Aro, E.M. and Morosinotto, T. (2016) Flavodiiron proteins act as safety valve for electrons in Physcomitrella patens. *Proc. Natl. Acad. Sci. USA*, **113**, 12322–12327. https://doi.org/10.1073/pnas.1606685113

Gómez, R., Carrillo, N., Morelli, M.P., Tula, S., Shahinnia, F., Hajirezaei, M.R. and Lodeyro, A.F. (2018) Faster photosynthetic induction in tobacco by expressing cyanobacterial flavodiiron proteins in chloroplasts. *Photosynth. Res.* **146**, 129–136.

Guo, J., Nguyen, A.Y., Dai, Z. *et al.* (2014) Proteome-wide light/dark modulation of thiol oxidation in cyanobacteria revealed by quantitative site-specific redox proteomics. *Mol. Cell Proteomics*, **13**, 3270–3285.

Hanke, G.T., Satomi, Y., Shinmura, K., Takao, T. and Hase, T. (2011) A screen for potential ferredoxin electron transfer partners uncovers new, redox dependent interactions. *Biochim. Biophys. Acta Proteins Proteomics*, **1814**, 366–374.

Han, X., Sun, N., Xu, M. and Mi, H. (2017) Co-ordination of NDH and Cup proteins in CO2 uptake in cyanobacterium Synechocystis sp PCC 6803. *J. Exp. Bot.* **68**, 3869–3877. https://doi.org/10.1093/jxb/erx129

He, Z., Zheng, F., Wu, Y., Li, Q., Lv, J., Fu, P. and Mi, H. (2015) NDH-1L interacts with ferredoxin via the subunit NdhS in Thermosynechococcus elongatus. *Photosynth. Res.* **126**, 341–349. https://doi.org/10.1007/s11120-015-0090-4

Helman, Y., Tchernov, D., Reinhold, L., Shibata, M., Ogawa, T., Schwarz, R., Ohad, I. and Kaplan, A. (2003) Genes encoding A-type flavoproteins are essential for photoreduction of O_2 in cyanobacteria. *Curr. Biol.* **13**(3), 230–235. https://doi.org/10.1016/S0960-9822(03)00046-0

Holland, S.C., Kappell, A.D. and Burnap, R.L. (2015) Redox changes accompanying inorganic carbon limitation in Synechocystis sp. PCC 6803. *Biochim. Biophys. Acta*, **1847**, 355–363. https://doi.org/10.1016/j.bbabio.2014.12.001

Ilik, P., Pavlovic, A., Kouril, R., Alboresi, A., Morosinotto, T., Allahverdiyeva, Y., Aro, E.M., Yamamoto, H. and Shikanai, T. (2017) Alternative electron transport mediated by flavodiiron proteins is operational in organisms from cyanobacteria up to gymnosperms. *New Phytol.* **214**(3), 967–972. https://doi.org/10.1111/nph.14536

Jokel, M., Johnson, X., Peltier, G., Aro, E.M. and Allahverdiyeva, Y. (2018) Hunting the main player enabling Chlamydomonas reinhardtii growth under fluctuating light. *Plant J.* **94**, 822–835. https://doi.org/10.1111/tpj.13897

Jokel, M., Nagy, V., Tóth, S.Z., Kosourov, S. and Allahverdiyeva, Y. (2019) Elimination of the flavodiiron electron sink facilitates long-term H2 photoproduction in green algae. *Biotechnol. Biofuels*, **12**, 280. https://doi.org/10.1186/s13068-019-1618-1

Kaplan, A. and Reinhold, L. (1999) CO_2 concentrating mechanisms in photosynthetic microorganisms. *Annu. Rev. Plant Physiol. Plant Mol. Biol.* **50**, 539–570. https://doi.org/10.1146/annurev.arplant.50.1.539

Kauny, J. and Setif, P. (2014) NADPH fluorescence in the cyanobacterium Synechocystis sp PCC 6803: a versatile probe for in vivo measurements of rates, yields and pools. *Biochim. Biophys. Acta Bioenerg.* **1837**, 792–801. https://doi.org/10.1016/j.bbabio.2014.01.009

Klughammer, C. and Schreiber, U. (2008) Saturation Pulse method for assessment of energy conversion in PSI. *PAM Application Notes*, **1**, 11–14.

Klughammer, C. and Schreiber, U. (2016) Deconvolution of ferredoxin, plastocyanin, and P700 transmittance changes in intact leaves with a new type of kinetic LED array spectrophotometer. *Photosynth. Res.* **128**, 195–214.

Kramer, D.M., Avenson, T.J. and Edwards, G.E. (2004) Dynamic flexibility in the light reactions of photosynthesis governed by both electron and proton reactions. *Trends Plant Sci.* **9**, 349–357.

Laughlin, T.G., Bayne, A.N., Trempe, J.F., Savage, D.F. and Davies, K.M. (2019) Structure of the complex I-like molecule NDH of oxygenic photosynthesis. *Nature*, **566**, 411–414.

Liran, O., Shemesh, E. and Tchernov, D. (2018) Investigation into the CO_2 concentrating step rates within the carbon concentrating mechanism of Synechocystis sp PCC6803 at various pH and light intensities reveal novel mechanistic properties. *Algal Res.* **33**, 419–429. https://doi.org/10.1016/j.algal.2018.06.020

Liu, L., Bryan, S.J., Huang, F., Yu, J., Nixon, P.J., Rich, P.R. and Mullineaux, C.W. (2012) Control of electron transport routes through redox-regulated redistribution of respiratory complexes. *Proc. Natl. Acad. Sci. USA*, **109**, 11431–11436. https://doi.org/10.1073/pnas.1120960109

Mehler, A.H. (1957) Studies on reactions of illuminated chloroplasts. I. Mechanism of the reduction of oxygen and other Hill reagents. *Arch. Biochem. Biophys.* **33**, 65–77.

Ma, W. and Ogawa, T. (2015) Oxygenic Photosynthesis-specific Subunits of Cyanobacterial NADPH Dehydrogenases. *IUBMB Life*, **67**, 3–8. https://doi.org/10.1002/iub.1341

McCormick, A.J., Bombelli, P., Lea-Smith, D.J., Bradley, R.W., Scott, A.M., Fisher, A.C., Smith, A.G. and Howe, C.J. (2013) Hydrogen production through oxygenic photosynthesis using the cyanobacterium Synechocystis sp PCC 6803 in a bio-photoelectrolysis cell (BPE) system. *Energy Environ. Sci.* **6**, 2682–2690. https://doi.org/10.1039/c3ee40491a

Michelet, L., Zaffagnini, M., Morisse, S. *et al.* (2013) Redox regulation of the Calvin-Benson cycle: something old, something new. *Front. Plant Sci.* **25**, 470. https://doi.org/10.3389/fpls.2013.00470

Mullineaux, C.W. (2014) Co-existence of photosynthetic and respiratory activities in cyanobacterial thylakoid membranes. *Biochim. Biophys. Acta Bioenerg.* **1837**, 503–511. https://doi.org/10.1016/j.bbabio.2013.11.017

Mustila, H., Paananen, P., Battchikova, N., Santana-Sanchez, A., Muth-Pawlak, D., Hagemann, M., Aro, E.M. and Allahverdiyeva, Y. (2016) The Flavodiiron protein Flv3 functions as a Homo-Oligomer during stress acclimation and is distinct from the Flv1/Flv3 Hetero-Oligomer specific to the O-2 photoreduction pathway. *Plant Cell Physiol.* **57**, 1468–1483. https://doi.org/10.1093/pcp/pcw047

Nakamura, Y., Kaneko, T., Miyajima, N. and Tabata, S. (1999) Extension of CyanoBase. CyanoMutants: repository of mutant information on *Synechocystis* sp strain PCC6803. *Nucleic Acids Res.* **27**, 66–68. https://doi.org/10.1093/nar/27.1.66

Nikkanen, L., Toivola, J., Trotta, A., Guinea Diaz, M., Tikkanen, M., Aro, E.M. and Rintamäki, E. (2018) Regulation of cyclic electron flow by chloroplast NADPH-dependent thioredoxin system. *Plant Direct*, **2**, 1–24.

Ogawa, T. (1991) A gene homologous to the subunit-2 gene of NADH dehydrogenase is essential to inorganic carbon transport of Synechocystis PCC6803. *Proc. Natl. Acad. Sci. USA*, **88**, 4275–4279.

Ohkawa, H., Price, G.D., Badger, M.R. and Ogawa, T. (2000a) Mutation of ndh genes leads to inhibition of CO_2 uptake rather than HCO_3^- uptake in Synechocystis sp. strain PCC 6803. *J. Bacteriol.* **182**(9), 2591–2596. https://doi.org/10.1128/JB.182.9.2591-2596.2000

Ohkawa, H., Pakrasi, H.B. and Ogawa, T. (2000b) Two types of functionally distinct NAD(P)H dehydrogenases in *Synechocystis* sp strain PCC6803. *J. Biol. Chem.* **275**, 31630–31634. https://doi.org/10.1074/jbc.M003706200

Peltier, G., Aro, E.M. and Shikanai, T. (2016) NDH-1 and NDH-2 Plastoquinone reductases in oxygenic photosynthesis. *Annu. Rev. Plant Biol.* **67**, 55–80.

Santana-Sanchez, A., Solymosi, D., Mustila, H., Bersanini, L., Aro, E.M. and Allahverdiyeva, Y. (2019) Flavodiiron proteins 1–to-4 function in versatile combinations in O_2 photoreduction in cyanobacteria. *eLife*, **8**, e45766. https://doi.org/10.7554/eLife.45766

Saura, P. and Kaila, V.R.I. (2019) Molecular dynamics and structural models of the cyanobacterial NDH-1 complex. *Biochim. Biophys. Acta Bioenerg.* **1860**, 201–208. https://doi.org/10.1016/j.bbabio.2018.11.010

Schreiber, U. and Klughammer, C. (2009) New NADPH/9-AA module for the DUAL-PAM-100: description, operation and examples of application. *PAM Application Notes*, **2**, 1–13.

Schreiber, U. (2017) Redox changes of ferredoxin, P700, and plastocyanin measured simultaneously in intact leaves. *Photosynth. Res.* **134**, 343–360.

Schuller, J.M., Birrell, J.A., Tanaka, H. *et al.* (2019) Structural adaptations of photosynthetic complex I enable ferredoxin-dependent electron transfer. *Science*, **363**, 257–260. https://doi.org/10.1126/science.aau3613

Setif, P., Boussac, A. and Krieger-Liszkay, A. (2019) Near-infrared in vitro measurements of photosystem I cofactors and electron-transfer partners with a recently developed spectrophotometer. *Photosynth. Res.* **142**, 307–319. https://doi.org/10.1007/s11120-019-00665-2

Shibata, M., Ohkawa, H., Kaneko, T., Fukuzawa, H., Tabata, S., Kaplan, A. and Ogawa, T. (2001) Distinct constitutive and low-CO2-induced CO2

uptake systems in cyanobacteria: genes involved and their phylogenetic relationship with homologous genes in other organisms. *Proc. Natl. Acad. Sci. USA*, **98**, 11789–11794. https://doi.org/10.1073/pnas.191258298

Shibata, M., Katoh, H., Sonoda, M., Ohkawa, H., Shimoyama, M., Fukuzawa, H., Kaplan, A. and Ogawa, T. (2002) Genes essential to sodium-dependent bicarbonate transport in cyanobacteria - Function and phylogenetic analysis. *J. Biol. Chem.* **277**, 18658–18664. https://doi.org/10.1074/jbc.M112468200

Shimakawa, G., Shaku, K., Nishi, A., Hayashi, R., Yamamoto, H., Sakamoto, K., Makino, A., Miyake, C. (2015) FLAVODIIRON2 and FLAVODIIRON4 proteins mediate an oxygen-dependent alternative electron flow in Synechocystis sp. PCC 6803 under CO_2-limited conditions. *Plant Physiol.* **167**(2), 472–480. https://doi.org/10.1104/pp.114.249987

Shimakawa, G., Shaku, K. and Miyake, C. (2016) Oxidation of P700 in Photosystem I is essential for the growth of cyanobacteria. *Plant Physiol.* **172** (3), 1443–1450. https://doi.org/10.1104/pp.16.01227

Shimakawa, G. and Miyake, C. (2018a) Changing frequency of fluctuating light reveals the molecular mechanism for P700 oxidation in plant leaves. *Plant Direct*, **2**, e00073.

Shimakawa, G. and Miyake, C. (2018b) Oxidation of P700 ensures robust photosynthesis. *Front. Plant Sci.* **9**, 1617. https://doi.org/10.3389/fpls.2018.01617

Strand, D.D., D'Andrea, L. and Bock, R. (2019) The plastid NAD(P)H dehydrogenase-like complex: structure, function and evolutionary dynamics. *Biochem. J.* **476**, 2743–2756. https://doi.org/10.1042/BCJ20190365

Strand, D.D., Fisher, N. and Kramer, D.M. (2017) The higher plant plastid NAD(P)H dehydrogenase-like complex (NDH) is a high efficiency proton pump that increases ATP production by cyclic electron flow. *J. Biol. Chem.* **292**, 11850–11860.

Thiel, K., Patrikainen, P., Nagy, C., Fitzpatrick, D., Pope, N., Aro, E.M. and Kallio, P. (2019) Redirecting photosynthetic electron flux in the cyanobacterium Synechocystis sp. PCC 6803 by the deletion of flavodiiron protein Flv3. *Microb. Cell Fact.* **18**, 189. https://doi.org/10.1186/s12934-019-1238-2

Tiwari, A., Mamedov, F., Grieco, M., Suorsa, M., Jajoo, A., Styring, S., Tikkanen, M. and Aro, E.M. (2016) Photodamage of iron-sulphur clusters in photosystem I induces non-photochemical energy dissipation. *Nat. Plants*, **2**, 16035.

Ueda, M., Kuniyoshi, T., Yamamoto, H., Sugimoto, K., Ishizaki, K., Kohchi, T., Nishimura, Y. and Shikanai, T. (2012) Composition and physiological function of the chloroplast NADH dehydrogenase-like complex in Marchantia polymorpha. *Plant J.* **72**, 683–693. https://doi.org/10.1111/j.1365-313X.2012.05115.x

Vicente, J.B., Gomes, C.M., Wasserfallen, A. and Teixeira, M. (2002) Module fusion in an A-type flavoprotein from the cyanobacterium Synechocystis condenses a multiple-component pathway in a single polypeptide chain. *Biochem. Biophys. Res. Commun.* **294**, 82–87. https://doi.org/10.1016/S0006-291X(02)00434-5

Viola, S., Bailleul, B., Yu, J., Nixon, P., Selles, J., Joliot, P. and Wollman, F. (2019) Probing the electric field across thylakoid membranes in cyanobacteria. *Proc. Natl. Acad. Sci. USA*, **116**, 21900–21906. https://doi.org/10.1073/pnas.1913099116

Williams, J.G.K. (1988) Construction of specific mutations in Photosystem-li Photosynthetic reaction center by genetic-engineering methods in Synechocystis-6803. *Meth. Enzymol.* **167**, 766–778.

Xu, M., Bernát, G., Singh, A., Mi, H., Rögner, M., Pakrasi, H.B. and Ogawa, T. (2008) Properties of mutants of Synechocystis sp. strain 6803 lacking inorganic carbon sequestration systems. *Plant Cell Physiol.* **49**, 1672–1677. https://doi.org/10.1093/pcp/pcn139

Yamamoto, H., Takahashi, S., Badger, M.R. and Shikanai, T. (2016) Artificial remodelling of alternative electron flow by flavodiiron proteins in Arabidopsis. *Nat. Plants*, **2**, 16012. https://doi.org/10.1038/nplants.2016.12

Yamori, W., Sakata, N., Suzuki, Y., Shikanai, T. and Makino, A. (2011) Cyclic electron flow around photosystem I via chloroplast NAD(P)H dehydrogenase (NDH) complex performs a significant physiological role during photosynthesis and plant growth at low temperature in rice. *Plant J.* **68**, 966–976.

Yamori, W., Shikanai, T. and Makino, A. (2015) Photosystem I cyclic electron flow via chloroplast NADH dehydrogenase-like complex performs a physiological role for photosynthesis at low light. *Sci. Rep.* **5**, 15593.

Yamori, W. and Shikanai, T. (2016) Physiological functions of cyclic electron transport around photosystem I in sustaining photosynthesis and plant growth. *Annu. Rev. Plant Biol.* **67**, 81–106.

Yeremenko, N., Jeanjean, R., Prommeenate, P., Krasikov, V., Nixon, P.J., Vermaas, W., Havaux, M. and Matthijs, H. (2005) Open reading frame ssr2016 is required for antimycin A-sensitive photosystem I-driven cyclic electron flow in the cyanobacterium Synechocystis sp PCC 6803. *Plant Cell Physiol.* **46**, 1433–1436. https://doi.org/10.1093/pcp/pci147

Zhang, P., Battchikova, N., Jansen, T., Appel, J., Ogawa, T. and Aro, E.M. (2004) Expression and functional roles of the two distinct NDH-1 complexes and the carbon acquisition complex NdhD3/NdhF3/CupA/Sll1735 in Synechocystis sp PCC 6803. *Plant Cell*, **16**, 3326–3340. https://doi.org/10.1105/tpc.104.026526

Zhang, P., Allahverdiyeva, Y., Eisenhut, M. and Aro, E.M. (2009) Flavodiiron proteins in oxygenic photosynthetic organisms: photoprotection of Photosystem II by Flv2 and Flv4 in Synechocystis sp PCC 6803. *PLoS ONE*, **4**, e5331. https://doi.org/10.1371/journal.pone.0005331

Zhao, J., Gao, F., Fan, D.Y., Chow, W.S. and Ma, W. (2017) NDH-1 is important for Photosystem I function of Synechocystis sp. strain PCC 6803 under environmental stress conditions. *Front. Plant Sci.* **8**, 2183. https://doi.org/10.3389/fpls.2017.02183